Modelling, Simulation, and Multi-Objective Optimisation of an Industrial Hydrocracking Unit

3 AUTHORS:

Naveen Bhutani

ABB Limited

7 PUBLICATIONS **58** CITATIONS

SEE PROFILE

Ajay Ray

The University of Western Ontario

175 PUBLICATIONS **4,989** CITATIONS

SEE PROFILE

Gade Pandu Rangaiah

National University of Singapore

240 PUBLICATIONS **2,389** CITATIONS

SEE PROFILE

Modeling, Simulation, and Multi-objective Optimization of an Industrial Hydrocracking Unit

Naveen Bhutani, Ajay K. Ray, and G. P. Rangaiah*

Department of Chemical & Biomolecular Engineering, National University of Singapore, 4 Engineering Drive 4, Singapore 117576

Hydrocracking is a petroleum refining process where cracking occurs simultaneously with hydrogenation to convert heavy petroleum feedstocks into desired lighter products. In this study, multi-objective optimization of an industrial hydrocracking unit has been performed for the first time, to find scope for further improvements and to provide a range of optimal solutions. The reactor model was simulated based on a discrete lumped model approach to kinetic modeling. The kinetic and product distribution parameters were fine-tuned using available industrial data. The real-coded elitist nondominated sorting genetic algorithm was used to carry out the multi-objective optimization study. The Pareto-optimal solutions for the hydrocracker unit are presented, and their significant features are discussed.

Introduction

Hydrocracking is a catalytic cracking process for the conversion of complex feedstock like heavy vacuum gas oils into more valuable lower boiling products, such as gasoline, kerosene, and diesel, in hydrogen-rich atmosphere at elevated temperature and pressure.[1] The reactions that occur in hydrocracking are cracking of the high molecular weight compounds giving rise to low molecular weight compounds and hydrogenation of olefins, aromatic rings, and sulfur, nitrogen, and oxygen compounds to some extent. The cracking reaction provides the olefins for hydrogenation, while the hydrogenation liberates the heat required for cracking. The cracking reactions are slightly endothermic while the hydrogenation reactions are highly exothermic, making the overall hydrocracking process highly exothermic in nature. Hydrocracking is the best source of low-sulfur and low-aromatics diesel fuel as well as high-smoke-point jet fuel. The higher hydrogen content of the products provides better combustion characteristics, making hydrocracking technology necessary to meet the current and future fuel specifications. Moreover, hydrocracking has the capability of processing a wide range of feedstocks of different characteristics to produce a broad range of products.

Even though considerable amount of research has been reported on reaction mechanism, catalysts, kinetic modeling, hydrodynamics, and reactor simulation of hydrocrackers, hardly any work on the optimization, either single or multiple objectives, of hydrocracking units has been reported in the open literature. Due to increasing worldwide demand for jet fuel and diesel and the easy availability of H_2 from the catalytic reforming unit within the plant premises, the hydroprocessing industry has considerable growth potential. Although hydrocracking technology is quite advanced, new developments in catalyst and changes in reactor design influence the operation of the entire unit. This requires attention to optimize catalyst design, minimize utility consumption, and to have the best resource utilization. Multiple objectives are relevant in such cases. In multi-objective optimization,[2−4] a solution that is the best (global optimum) with respect to all objectives may not exist. Instead, an entire set of optimal solutions that are equally good could exist. These solutions are known as Pareto-optimal (or nondominated) solutions.

The present work employs a discrete lumped model approach[5] to modeling an industrial hydrocracker and its simulation. The first principle reactor model was fine-tuned for its kinetic and product distribution parameters using steady-state plant data. The model was then validated and used to analyze the behavior of an industrial unit with respect to a number of variables. Finally, the hydrocracker unit was optimized using the validated model and a real-coded nondominated sorting genetic algorithm[4] (NSGA, an adapted version of a genetic algorithm suitable for multi-objective problems) for industrially important objectives and operational constraints. The present work is the first attempt to study optimization of an industrial hydrocracking unit for multiple objectives. Apart from this main contribution, other contributions of this work are on modeling and simulation of the industrial hydrocracker (HC): (a) parameter estimation through optimization; (b) use of recent and new data from an industrial HC unit; and (c) successful application of the refined model to another industrial HC unit.

Process Description

Hydroprocessing is carried out in packed bed catalytic reactors at elevated temperature and pressure for conversion of heavy oils to middle distillates in hydrogen-rich atmosphere. Since hydrocracking reactions involve both cracking and hydrogenation, they require dual functional catalysts[7] consisting of a hydrogenation component dispersed on a porous acidic support for providing cracking activity. A typical catalyst consists of silica−alumina (or low- or high-zeolite SiO_2−Al_2O_3) with base metal components such as Ni, Pt, Pd, W, and Mo. The silica−alumina portion promotes cracking activity, while the metals encourage hydrogenation. Hydrocracking is carried out in multiple catalyst beds under a trickle flow regime.[8] Usually, the process employs two reactors in series: a hydrotreater (HT) and a hydrocracker (HC), to accomplish hydrotreating in the first followed by hydrocracking in the latter. The fresh feed to a hydrotreater (heavy vacuum gas oil, HVGO) is a homogeneous mixture of various hydrocarbons classified as paraffins, olefins, aromatics, naphthenes, and structured-ring compounds. In addition to these, sulfur in the form of thiols, mercaptans, sulfides, disulfides, and thiophenes, nitrogen in the form of

* Corresponding author. Tel.: (65) 6516 2187. Fax: (65) 6779 1936. E-mail: chegpr@nus.edu.sg.
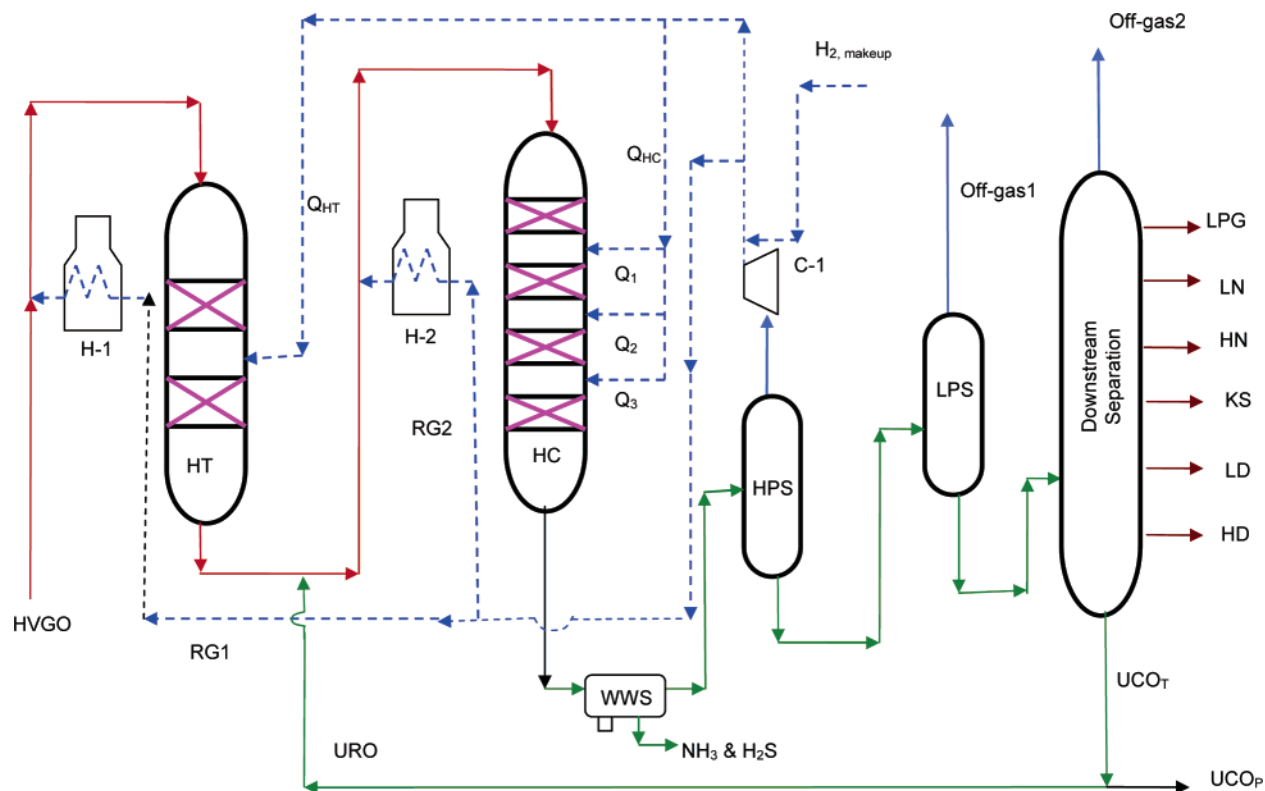
Figure 1. Simplified process flow diagram of the hydrocracking unit.

indoles, pyridines, quinolines, and amines, and metal compounds are also present.

The process flow diagram (without coolers, pumps, and heat exchangers for simplicity and proprietary reasons) is shown in Figure 1. The HT and HC consist of 2 and 4 beds, respectively, with quenching by recycle H_2 to cool the reaction mixture between the beds and control the reaction temperature. The feed to the hydrotreater is a mixture of HVGO (BP range 629−854 K) and recycled H_2 (RG1 in Figure 1) which are heated separately in fired heaters and heat exchangers to attain the required reaction temperature before they enter the reactor. The HT operates at relatively higher pressure and lower temperature (176.6 atm and 642 K) in comparison to the HC (170 atm and 672 K). In the HT, sulfur, nitrogen, and oxygen compounds are decomposed to hydrogen sulfide, ammonia, and water, while aromatics and olefins, if any, are hydrogenated. The flow of oil is once through and vertically downward. The catalyst used in the hydrotreater has a high hydrogenation/acidity ratio, causing mainly feed hydrogenation and mild hydrocracking.

The feed to the HC is a mixture of HT effluent, unconverted recycle oil (URO), and recycle gas (RG2). The feed is hydroisomerized and hydrocracked in the hydrocracker in the presence of a bifunctional catalyst loaded with noble metals. The hydrogenation/acidity ratio of the catalyst used depends on the product requirement. The once through conversion (X_{pass}) is 65−69 wt %, whereas overall conversion ($X_{overall}$) is 95−98 wt % on a product basis. The product mixture from the HC is cooled in a series of heat exchangers (not shown in Figure 1) by transferring thermal energy to URO, recycle H_2 gas, and HVGO. The product mixture contains a series of hydrocarbons ranging from C_1 (methane) to C_{32} and other products such as ammonia, hydrogen sulfide, and unreacted hydrogen.

The effluent from the HC is sent to a wash water separator (WWS) to remove most of the NH_3. A small but negligible amount of H_2S is lost during this process. The lightest component, hydrogen is separated in the high-pressure separator

(HPS). Light gases so recovered are almost 91 mol % pure H_2 and are compressed and mixed with makeup hydrogen ($H_{2,makeup}$). This gas is recycled back to the two reactors (HT and HC): some part (RG1 and RG2) is for mixing with their feed, and the remaining (Q_{HT} and Q_{HC}) is for quenching between the catalyst beds. H_2S is recovered from the low-pressure separator (LPS) gas and debutanizer off-gas (shown respectively as Off-gas1 and Off-gas2 in Figure 1) by downstream amine treatment and the Claus process. Some amount of H_2 is lost with these off-gases. The bottom liquid product from LPS is further cooled and sent to the downstream separation system consisting of a debutanizer (where lighter products—CH_4, C_2H_6, LPG, etc.— are recovered from the top) and two multicomponent distillation columns in series. The main products from these two columns are light naphtha (LN), heavy naphtha (HN), kerosene (KS), light diesel (LD), and heavy diesel (HD).

Hydrocracking Kinetics and Modeling

The kinetic model should ideally take into account all reactions that the components in the feedstock undergo. However, in reality, it is difficult to do so due to the complex chemistry of hydrocarbons in the feed and reaction mixture, numerous components and reactions, and the lack of kinetic data. Researchers have proposed two distinct classes of kinetic models: lumped and detailed molecular models. Lumped models have been based on discrete lumping, structure oriented lumping, or continuous lumping. In the discrete lumping approach, the individual components in the reaction mixture are divided into discrete pseudocompounds (lumps) based on the true boiling point (TBP), carbon number (CN), and/or molecular weight (MW). Instead of keeping track of individual molecules, the molecules with a similar CN, MW, or TBP group are treated as cracking with a particular rate constant to give predefined lower lumps. The classical examples for the discrete lumped approach are Weekman's 10-lump model[5] for fluid catalytic

cracking (FCC) and Stangeland's model[9] for hydrocracking. Subsequently, several discrete lumped models have been proposed to study the hydrocracking process.[10−13] The success of this approach depends on the choice of the number of lumps. A large number of lumps would result in more accurate predictions, but this increases the number of kinetic parameters that describe the system.

The concepts of detailed elementary reaction schemes[14] and theory of single event kinetics,[15] which led to structure oriented lumping,[16] have been proposed for modeling hydrotreating,[17] catalytic cracking, and hydrocracking processes. Quann and Jaffe[18,19] developed a detailed elementary reaction scheme concept of structure oriented lumping in order to reduce the number of reactions involved. The theory of a single event kinetic model has been applied to simulate the hydrocracking of paraffins in a three-phase reactor.[15] This approach requires a large amount of experimental data and computational power to build a reasonable model. Martens and Marin[20] developed fundamental kinetic approaches such as single-event kinetic models based on structural classes by incorporating carbonium ion chemistry in order to reduce the large data requirement, excessive computational time, and memory capacity. The reaction rate coefficient for reactions was determined by partial relumping of the single event kinetics equations.[21]

The continuous lumping approach considers the reactive mixture to form a continuum mixture with respect to its species type, TBP, MW, etc. Research in this direction had been carried out by several researchers.[22−26] Application of the continuous theory of lumping has been described for hydrocracking of vacuum gas oil[27−29] in which measurable quantities such as TBP were used as characterization parameters for continuous lumping and describing the reaction rates and physical properties. This continuous treatment of complex mixtures results in a partial integral−differential equation.[30] The continuous theory of lumping can also improve structure oriented lumping.

The main issues that refiners have to deal with in the daily operation of the plant are product yield and quality, reactor temperature, and the makeup hydrogen requirement. The studies of Mohanty et al.[13] and Pacheco and Dassori[31] show that the discrete lumped model approach is capable of predicting these quantities satisfactorily. Moreover, such a model can easily be implemented even when the experimental data is limited and feed quality changes, whereas detailed kinetic models based on molecular reaction schemes need accurate feed analysis. Hence, the discrete lumped model approach is chosen for simulating and optimizing an industrial hydrocracker for multiple objectives. The specific model adopted for this study is that of Mohanty et al.,[13] which is based on the kinetic model of Stangeland.[9] Pacheco and Dassori[31] noted that this kinetic model has been widely used in the fuel processing industry.

Modeling and Simulation of the Hydrocracking Unit

The HC unit consists of two main sections: a reactor section and a separation section. The two reactors—HT and HC—in the reactor section are simulated using a simplified model for the HT and a first principles model for the HC. The separation section consisting of WWS, HPS, LPS, and a downstream section (Figure 1) is simulated using a black-box model. This is a practical approach and is yet satisfactory because the HC model is the most critical for simulating the HC unit.

The main reactions in the HT are hydrodesulfurization (HDS) and hydrodenitrogenation (HDN) reactions, which consume hydrogen. The rigorous simulation of the HT is beyond the scope of this work. To estimate the effluent gas composition from

the HT and the hydrogen consumption in it, the consumption of H_2 for HDS and HDN is based on the stoichiometry of reaction for the model sulfur and nitrogen compounds, namely, benzothiophene and quinoline, respectively. Nitrogen and sulfur content in the liquid at the inlet and exit of the HT are known. The quantity of light components other than H_2, H_2S, and NH_3 is assumed to be constant throughout the HT. On the basis of these assumptions and known quantities, gas composition at the HT exit is estimated. Using this estimated composition and the known composition of RG2, the composition of mixed gas to the HC is then evaluated (Figure 1).

In the industry, the HT liquid effluent is only analyzed for the nitrogen and sulfur content and for the density. Hence, its characterization to pseudocomponents and their property estimation is impossible. Therefore, the pseudocomponent composition of the HT effluent liquid is assumed to be the same as that of the feed (HVGO). The molecular size distribution of pseudocomponents does not change much due to mild hydrocracking[32] in the HT. The slight discrepancies that may arise due to mild hydrocracking are taken into account in the subsequent fine-tuning of the HC model parameters.

Hydrocracking is performed in multiphase, multiple fixed-bed, multicatalytic reactors. The liquid phase consists of hydrocarbon feed, the gas phase consists of hydrogen and evaporated feed components, while the catalyst makes up the solid phase. In modeling the HC, it is necessary to account for the yield and selectivity of various products.[30] Stangeland[9] found that heavier cuts crack via a first-order mechanism to form smaller/lighter cuts. To describe the effect of the boiling point on the rate constant and the amount of product generated, he[9] followed a three-parameter approach. One parameter describes the effect of the boiling point on the rate constant and the other two parameters determine the product yield. Mohanty et al.[13] adopted this three-parameter model for the simulation of a two-stage vacuum gas oil HC unit. Pacheco and Dassori[31] developed an improved kinetic model with two additional parameters and a mass balance closure for each hydrocracking reaction, which Mohanty et al.[13] had not considered. However, the latter took care of overall mass balance enclosure by calculating hydrogen consumption in the reactor.

The model of Pacheco and Dassori[31] was based on regression analysis of kinetic parameters to satisfy mass balance enclosure for each hydrocracking reaction using the Levenberg−Marquardt algorithm. They have implemented it using the default reactor model, RPLUG in the AspenPlus simulator. However, the predicted temperature profile does not match with that reported by Mohanty et al.[13] or with the expected trend for HCs with intermediate cooling (e.g., see Figure 2 for the industrial HC simulated in this study). Following the guidelines and concepts proposed by researchers,[9,13,31] this study simulates an industrial HC unit employing the first principles model based on a discrete lumped model approach along with empirical correlations for kinetics and product distribution. This is described below.

The HC is modeled assuming plug flow, negligible diffusional resistances, and adiabatic and steady-state conditions. Further, HDS and HDN reactions in the HC and the amount of quench added at the HC inlet (not shown in Figure 1) are assumed to be negligible. The component mass balances for the liquid phase for a differential catalyst element in the HC is

$$M_t \frac{dC_i}{dW} = -k_i C_i + \sum_{j=r}^{N} k_j P_{ij} C_j \qquad i = 1 \text{ to } N,$$
$$r = i + 2 \text{ for } i \geq 13, \quad r = 14 \text{ for } i < 13 \quad (1)$$
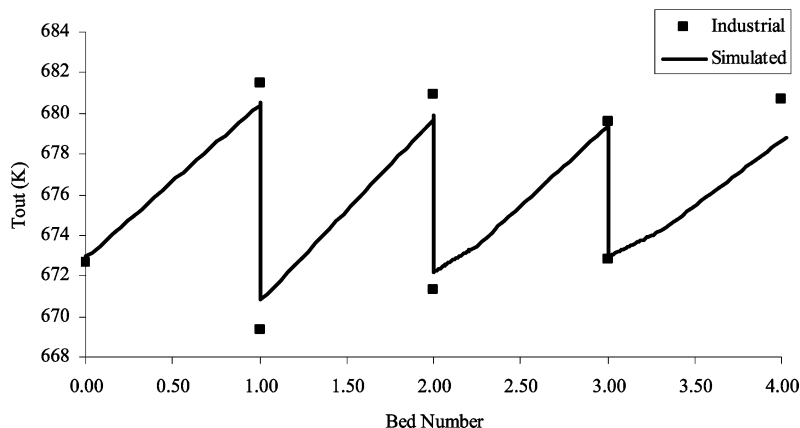
Figure 2. Comparison of simulated (model prediction) and industrial temperature profiles.

The first term on the right-hand side in eq 1 denotes the disappearance of pseudocomponent i and is zero when $i \leq 13$ because these lighter components (with a boiling point less than 400 K) are assumed not to crack. The second term denotes the rate of formation of the ith component from higher components (starting from the $i+2$th component). In eq 1, N is the highest hydrocarbon being cracked, P_{ij} is the probability of formation of the ith pseudocomponent from the jth pseudocomponent by cracking, M_t is the total mass flow rate of liquid feed to the catalyst bed in kg/h, C_i is the mass fraction of the ith pseudocomponent, and k_i is the first-order rate constant for cracking of the ith pseudocomponent in kg-reactant/(kg-catalyst h). Note that M_t is assumed to be constant across each bed.

The rate of hydrocracking depends on the hydrogen concentration, but hydrogen is present in large excess and is practically constant in industrial HCs. For example, the hydrogen mole fraction in the gas phase in the HC studied in this work varies between 0.92 and 0.90. Hence, it is acceptable to express the reaction rate without hydrogen partial pressure as in eq 1. Mass balance enclosure is, however, ensured by calculating the consumption of H_2 for all reactions in each differential catalyst element based on the flow rates of pseudocomponents and their C/H ratios.

The rate constant (k_i) for a particular pseudocomponent is highly dependent on the type of hydrocarbon feed and catalyst. Several kinetic studies have been published, but their application becomes limited due to different reaction conditions and the catalyst used. Hence, Mohanty et al.[13] assumed a simple form of the rate expression in which k_i for ith pseudocomponent is a product of a relative rate function (K_i) and an estimated rate constant (k) for the mixture with an average boiling point of 638 K.

$$k_i = K_i k \quad \text{where} \quad k = \left(\frac{\rho_{HVGO}}{\rho_{catalyst}}\right) A e^{-E/RT} \quad (2)$$

Quader and Hill[10] reported values of A and E as 1.0×10^7 volume of feed/(volume of catalyst h) and 21 100 kcal/kmol, respectively, for hydrocracking of a vacuum gas oil having a boiling range of 573−703 K. (The ratio of densities in the above equation is because of different units for k and A.) As a first estimate, these values were taken and later adjusted to predict the particular industrial data. The function K_i was developed based on the work of Rapaport,[45] who reported relative rates for hydrocracking of normal alkanes, found that the rate

increased in the ratio 1/32/72/120 for $C_5/C_{10}/C_{15}/C_{20}$, and reported an empirical polynomial for K_i:

$$K_i = D_1 + D_2 T_{b,i} + D_3 T_{b,i}^2 + D_4 T_{b,i}^3 \quad (3)$$

The values of the coefficients D_1-D_4 in this equation are obtained by matching the predictions with the plant data.

The product distribution during hydrocracking of each pseudocomponent was evaluated using correlations.[9] The mass fraction of butanes and lighter components formed from hydrocracking of jth pseudocomponent (with boiling point, T_{bj} in °C) is given by

$$P_{1j} = C \exp[-\omega(1.8 T_{bj} - 229.5)] \quad (4)$$

where C and ω are constants. The yield of all other fractions having boiling points higher than that of butane are evaluated using

$$P'_{ij} = [y_{ij}^2 + B(y_{ij}^3 - y_{ij}^2)][1 - P_{1j}] \quad (5)$$

where P'_{ij} is the cumulative products yield until the ith pseudocomponent from hydrocracking of the jth pseudocomponent. In the above equation, y_{ij} is the normalized temperature for the ith product formed from the jth pseudocomponent and is given by

$$y_{ij} = \frac{(T_{bi} - 2.5)}{[(T_{bj} - 20) - 2.5]} \quad \text{for } i = 2 \text{ to } j - 2, j = 14 \text{ to } N \quad (6)$$

The parameters, B and C, in eqs 4 and 5 depend on the paraffin content in the feed and the type of catalyst (Mohanty et al.[13]). The adjusted values of these parameters were obtained by matching predictions with the industrial data (see eq 9 given later). The yield of pseudocomponent i from component j is obtained from

$$P_{ij} = P'_{ij} - P'_{i-1,j} \quad (7)$$

The energy balance for a differential catalyst element in the HC is

$$\sum_i^{N+1} M_i C_{pi} \frac{dT}{dW} = \sum_j^N (-\Delta H)_{Rj} k_j C_j$$
$$i = 1 \text{ to } N + 1, j = 14 \text{ to } N \quad (8)$$

Here, the $(N+1)$th component is hydrogen, M_i is the mass flow

rate of the *i*th pseudocomponent (in kg/h), $(-\Delta H)_{Rj}$ is the heat of reaction for hydrocracking of the *j*th pseudocomponent in kcal/kg of hydrocarbon, C_{pi} is the heat capacity of component *i* (in kcal/(kg K)), and *T* is the temperature (in K). The heat of reaction at reaction conditions, $(-\Delta H)_{Rj}$, is evaluated as the sum of the standard heat of reaction, $(-\Delta H°)_{Rj}$, and difference in enthalpy of products and reactants at reaction conditions. Calculation of $(-\Delta H°)_{Rj}$ is discussed later in the Property Prediction section. In eqs 1 and 8, all pseudocomponents are assumed to exist in the liquid phase and no gas–liquid equilibrium calculations were performed for reactor simulation. Although some hydrogen is dissolved in the liquid phase, its quantity is very small (about 1% of total hydrogen present). Hence, for the energy balance, hydrogen is assumed to be totally in the gas phase. The temperature of the gas and liquid phases at any axial position in the reactor is assumed to be the same.

The above HC model is used to simulate hydrocracking of HVGO in each catalyst bed to predict the yield of pseudocomponents and H_2 consumption. At the end of each bed, the total mass of the liquid reaction mixture is evaluated as the sum of the liquid feed to the catalyst bed and the H_2 consumed in reactions. The difference in the liquid mass flow rates at the inlet and exit of each bed is less than 0.5%, which justifies the assumption of constant M_t for each bed (eq 1). The pseudocomponent mass flow rate at the bed exit is then evaluated as the product of the mass fraction of pseudocomponent (C_i) and the total mass of the liquid reaction mixture.

The temperature rise in the catalyst beds due to exothermic reactions is controlled by adding quench gas (Q_1, Q_2, and Q_3) between the beds. The enthalpy of quench gas is calculated based on its composition and average C_p values of the pure components present in the gas stream at operating temperature and pressure, obtained using Hysys. The inlet temperature of the gas and liquid mixture to the subsequent reactor bed is estimated using the enthalpy of the liquid reaction mixture at the previous bed exit and that of the added quench gas stream.

The HC effluent is processed through several downstream units, which are assumed to operate under steady-state and are modeled as a black-box. Flow rates of industrial products from the downstream section are calculated using the pseudocomponent flow rates in the liquid effluent from the HC and are outlined in the next section. One of these products is UCO_T, part of which is recycled as URO (Figure 1). To begin the simulation of the HC unit, flow rate, composition, and temperature of the URO are initialized at the industrial values. The successive substitution method is used to iterate on the URO flow rate. It takes 10–15 iterations for convergence of these recycle loop calculations. After achieving convergence, the $H_{2,makeup}$ quantity is determined by the sum of the H_2 consumed in HT and HC and the H_2 lost in Off-gas1 and Off-gas2. For this, the amount of H_2 lost with the off-gases, which is 4–6% of $H_{2,makeup}$, is fixed at the industrial value. Also, for simulating the HC unit, the composition and flow rates of RG1, RG2, Q_{HT}, and Q_{HC} are fixed at their industrial values. However, flow rates of RG2 and Q_{HC} are taken as decision variables for optimization.

Feed and Product Characterization

The feed and products of the HC need to be divided into pseudocomponents (based on the selected lumping technique), which is called characterization and can be done using oil manager in Hysys. For the application of the discrete lumped model approach, a tradeoff between the number of pseudocomponents and their boiling range is often a good practice to get better model accuracy and efficiency and to avoid ambiguity

during component selection. In our study, the feed and products were defined into 58 pseudocomponents each with a 10 °C boiling range. Typical light-end (LE) components such as methane, ethane, propane, *i*-butane, and *n*-butane along with small amount of pentanes (<1 mol %) and hexanes (<0.2 mol %) as well as NH_3 and H_2S are formed during hydrotreating and hydrocracking. A mixture of all these light components (with the exception of H_2S and NH_3) was taken as pseudocomponent 1 even though pentanes and hexanes are not included in the definition of pseudocomponent 1.

The available experimental assay data, obtained by batch/simulated distillation, for products were used to evaluate pseudocomponents composition of industrial products such as LPG (liquefied petroleum gas), LN, HN, KS, LD, HD, URO, and UCO_P. Since mass flow rates of these products were known, the mass flow rate of pseudocomponents present in each of these products could then be evaluated. Note that a pseudocomponent may exist in two different products in different fractions based on distillation efficiency (e.g., pseudocomponent 11, as shown in Table 1, is present in two products). Hence, the mass flow rate of pseudocomponents in each of the products was used to get a fractional distribution of each pseudocomponent to industrial products. Table 1 also gives the fractional distribution of pseudocomponents into products (e.g., the fractional distribution of pseudocomponent 11 to HN and LN is given as y_{HN} = 0.8498 and y_{LN} = 0.1502, which adds up to 1).

The process of feed and product characterization to pseudocomponents was automated by developing a macro in Excel. Since Hysys is object linking and embedding (OLE) compliant, its objects can be seen and accessed from outside applications such as Visual Basic and Excel. Table 1 gives the average properties of some pseudocomponents generated by feed and products characterization. It also includes the mass fraction of pseudocomponents in HVGO, HD, HN, and LN. Other pseudocomponents and products are not included in Table 1 for brevity.

Simulation of the HC unit gives flow rates of all pseudocomponents. To predict flow rates of LN, HN, KS, LD, HD, and UCO_T, we use these flow rates and the fractional distribution of pseudocomponents into products found by product characterization. Pseudocomponent 1 distributes into Off-gas1, Off-gas2, and LPG. As pure components in pseudocomponent 1 are not identified separately, it is not possible to predict Off-gas1, Off-gas2, and LPG individually. Hence, the actual flow rate of LE is calculated from industrial values of Off-gas1, Off-gas2, and LPG flow rates excluding H_2 and H_2S. The predicted flow rate of LE is simply that of pseudocomponent 1.

Property Prediction

The pseudocomponents obtained by characterization act as pure components and were defined by their weighted average mean properties such as boiling point and density (Table 1). Properties of pseudocomponents and their mixtures were estimated using empirical correlations available in the literature[32] as functions of normal boiling point and density. The empirical correlations of Lee and Kesler[33] were used for pseudocomponent properties such as molecular weight (MW), critical pressure (P_C), critical temperature (T_C), critical volume (V_C), and acentric factor (ω). For a mixture of these pseudocomponents, mixing rules were used.[34] To calculate the enthalpy and fugacity coefficient for a pseudocomponent and the partial fugacity coefficient, $\hat{\phi}_i$, Peng–Robinson cubic equation of state was used.[35] The ideal gas enthalpy of the pure component and mixture were evaluated using correlations given by Weir and Eaton.[36] The excess enthalpy for a pure component (or mixture)

Table 1. Characterization of Feed and Products into Pseudocomponents

component no.	TBP (°C)	ρ_{PC} (kg/m^3)	Watson K (−)	x_{HVGO} (−)	x_{HD} (−)	x_{HN} (−)	x_{LN} (−)	y_{HN} (−)	y_{LN} (−)
1	2.50	583.00	13.360	0.00	0.00	0.00	0.00	0.00	0.00
8	64.98	689.83	12.285	0.00	0.00	0.00	0.1580	0.0000	1.0000
9	74.60	701.12	12.201	0.00	0.00	0.0052	0.1287	0.0862	0.9138
10	84.33	712.33	12.120	0.00	0.00	0.0354	0.1292	0.3899	0.6101
11	94.62	721.87	12.073	0.00	0.00	0.1519	0.0626	0.8498	0.1502
12	103.98	730.67	12.028	0.00	0.00	0.1893	0.0421	0.9129	0.0871
13	114.79	740.95	11.974	0.00	0.00	0.1862	0.00	1.00	0.00
14	124.91	749.40	11.941	0.00	0.00	0.1586	0.00	0.9690	0.00
15	134.44	756.88	11.916	0.00	0.00	0.1314	0.00	0.8647	0.00
16	144.66	764.21	11.900	0.00	0.00	0.0915	0.00	0.00	0.00
17	154.28	769.62	11.906	0.00	0.00	0.0312	0.00	0.00	0.00
18	163.98	775.32	11.907	0.00	0.00	0.0194	0.00	0.00	0.00
36	344.93	858.67	12.067	0.00593	0.1175	0.00	0.00	0.00	0.00
37	354.78	861.94	12.085	0.00689	0.1028	0.00	0.00	0.00	0.00
38	365.11	866.48	12.087	0.00842	0.0957	0.00	0.00	0.00	0.00
39	375.33	872.26	12.071	0.01056	0.0931	0.00	0.00	0.00	0.00
40	385.25	877.61	12.058	0.01331	0.0874	0.00	0.00	0.00	0.00
41	395.25	882.49	12.052	0.01698	0.0772	0.00	0.00	0.00	0.00
49	475.03	915.61	12.061	0.06311	0.00	0.00	0.00	0.00	0.00
50	485.02	919.02	12.069	0.06525	0.00	0.00	0.00	0.00	0.00
51	494.99	922.20	12.080	0.06582	0.00	0.00	0.00	0.00	0.00
52	504.97	925.15	12.094	0.06513	0.00	0.00	0.00	0.00	0.00
53	514.95	927.84	12.110	0.06390	0.00	0.00	0.00	0.00	0.00
54	524.76	930.18	12.129	0.05874	0.00	0.00	0.00	0.00	0.00
55	535.06	932.25	12.154	0.05326	0.00	0.00	0.00	0.00	0.00
56	545.75	935.74	12.162	0.06563	0.00	0.00	0.00	0.00	0.00
57	553.59	938.47	12.165	0.03522	0.00	0.00	0.00	0.00	0.00
58	565.16	942.79	12.166	0.03452	0.00	0.00	0.00	0.00	0.00

Table 2. Experimental Data for Feed and Products Obtained from the Refinery^a

	feed	HT$_{Effluent}$	LN	HN	KS	LD	HD	UCO
IBP	310.00		34.70	101.10	163.90	199.20	305.20	315.50
5%	363.50		42.50	107.30	179.70	206.60	321.80	361.00
10%	383.50		46.80	109.00	183.50	219.00	326.00	380.50
20%	407.50		52.00	111.10	191.00			403.00
30%	424.50		56.50	113.60	198.10	227.80	333.00	417.50
40%								429.00
50%	456.50		65.00	119.10	216.00	244.60	342.40	440.50
60%								453.00
70%	487.00		73.20	126.60	237.80	258.00	356.00	467.00
80%	504.00							483.50
90%	526.50		85.10	138.00	263.70	272.20	373.40	507.00
95%	543.00		91.90	142.70	272.50	278.00	378.60	526.50
FBP	578.00		101.40	160.50	277.20	280.00	380.60	566.00
ρ (15 °C)	0.933	0.883	0.68	0.75	0.81	0.82	0.83	0.84
N$_2$ (ppm)	1413	64						7.20
S (wt %)	2.656	0.092		0.99		0.03		0.03

^{a} Note that the percent in column 1 refers to wt % for feed and UCO and to vol % for LN, HN, KS, LD, and HD. Boiling points in the table are in degrees Celsius.

was related to the fugacity coefficient by a thermodynamic relationship as described in ref 13.

The standard heat of reaction was calculated on the basis of the stoichiometric hydrogen requirement (Mohanty et al.[13]). It is given as the product of hydrogen consumed per unit amount of pseudocomponent j reacted and the amount of heat released per unit consumption of hydrogen, ($-\Delta H_{Hcon}$) in kcal/kmol. The former quantity can be calculated using the C/H ratio of pseudocomponents and P_{ij}. For ($-\Delta H_{Hcon}$), Mohanty et al.[13] assumed that 42 MJ of heat is released for each kmol of H$_2$ consumed. This agrees well with the standard heat of reaction for the hydrocracking of hexadecane.[37] The pseudocomponent composition of the HT effluent is assumed to be the same as that of HVGO feed to the HT, but the latter is hydrogenated in the HT, which is never analyzed. Hence, it is impossible to obtain the C/H ratio of the HT effluent and, subsequently, the C/H ratio of liquid feed to the HC. Hence, due to the unpredictability in the C/H ratio of the liquid feed to the HC, $-\Delta H_{Hcon}$ was fine-tuned in this work to match the measured temperatures at the bed exits.

The C/H ratio of hydrocarbons, required for estimating chemical consumption of H$_2$ in the HC, in the boiling point range of feed and products is tabulated in ref 38. These data were used to obtain correlations between the C/H ratio and the Watson characterization factor (Watson K). These correlations were used to find the hydrogen and carbon content of each pseudocomponent by interpolation based on the average boiling temperature of the pseudocomponent. Note that the value of Watson K for each pseudocomponent was obtained from Hysys.

With the availability of mass fraction of products (i.e., lighter pseudocomponents) from hydrocracking of each pseudocomponent and molecular weight and C/H ratio of all pseudocomponents, it is possible to calculate the hydrogen consumed in the reaction of each pseudocomponent and, thus, make the reaction balanced. The stoichiometric coefficients of this reaction can be calculated by converting the hydrogen consumed and the mass of products formed from hydrocracking of 1 mol of each pseudocomponent into moles. These, along with other property and kinetic data, can then be used in a process simulator for successfully simulating the hydrocracker.

Table 3. Data on Catalyst in the Hydrocracker Beds[a]

	HC					
	bed-1	bed-2	bed-3A	bed-3B	bed-4A	bed-4B
V_{cat}, m^3	22.70	25.00	5.6	20.3	7.2	18.2
M_{cat}, kg	19 997	23 586	4469	19 975	5738	17 800

[a] Two types of catalysts are present in bed 3 and bed 4, hence given as 3A and 3B and 4A and 4B.

Table 4. Set of Operating Data for Hydrotreater and Hydrocracker

operating data	HT	HC
F_{HVGO}, kL/h	a	
P_{inlet}, atm	176.60	170.54
T_{inlet}, K	655.99	672.25
T_{out}, K	689.72	680.04
Q_{HT}, Q_{HC}, tons/h	a	a
LHSV, 1/h		1.43
RG1, RG2, kg/h	a	a
T_{inlet1}, K		672.25
T_{out1}, K		680.89
T_{inlet2}, K		668.94
T_{out2}, K		680.27
T_{inlet3}, K		670.87
T_{out3}, K		679.04
T_{inlet4}, K		672.25
T_{out4}, K		680.04

[a] These data are not provided due to their confidential nature.

Model Calibration: Fine Tuning of Model Parameters

The simulation of a hydrocracker is very much dependent on feed properties, catalyst activity, reactor type, and operating conditions. Since the reactor configuration and operating conditions vary for different refineries, the fine-tuning of model parameters is essential. Numerous sets of the process and operation details, feed and product experimental data, and their flow rates for many days of operation over 3 months period, available from a local refinery, have been used in our HC unit simulation for model calibration and validation. The industrial data were verified for consistency (overall mass balance) before using for fine-tuning and model validation.

The sum of H$_{2,makeup}$ and HVGO is the total feed to the HC unit. The streams leaving the unit are Off-gas1, Off-gas2, LPG, LN, HN, KS, LD, HD, and UCO$_P$; the sum of these streams is the total product. (Ammonia formed in the HT leaves from the WWS, but this is small and neglected in the overall mass balance.) The difference between the total feed and total product indicates the consistency of the measured data. Those data, which were consistent within an error of ±5%, were accepted for model tuning and validation. This is justifiable considering the inevitable measurement errors in the data. The data consistency was carried out in an Excel spreadsheet. To automate the process of feed characterization and verification of data consistency, an experimental data sheet in Excel was interfaced with Hysys. The feed and products flow rates were taken from "User" through a graphical user interface developed in Excel.

The model of the HC unit described above and the subroutines for property estimation for simulating the process were coded in F90. The Runge−Kutta−Gill method was used to solve the differential equations for mass and energy balances. Typical feed properties, catalyst data, and process operating details are given in Tables 2−4. For all months of operation, the pseudo-components, which are defined by their average boiling point and density, representing the feed and products were kept the same. However, HVGO composition in terms of these pseudo-components varies. The HC unit was simulated using the plant operating values of HVGO flow rate, recycle gas temperature,

Table 5. Comparison of Fine Tuned Parameter Values Obtained in This Study with the Reported Values[13]

parameter	reported value[13]	tuned value
$-\Delta H_{Hcon}$, kcal/kmol	10 000	6310
A_1, vol feed/(vol cat h)	1.0×10^7	9.797×10^6
A_2, vol feed/(vol cat h)	1.0×10^7	9.952×10^6
A_3, vol feed/(vol cat h)	1.0×10^7	9.843×10^6
A_4, vol feed/(vol cat h)	1.0×10^7	9.844×10^6
D_1	0.494	0.5335
D_2	5.2×10^{-3}	5.616×10^{-3}
D_3	-2.185×10^{-5}	-2.425×10^{-5}
D_4	3.12×10^{-8}	3.37×10^{-8}
C	0.35	0.70
ω	0.01	0.02
B	0.70	0.64

recycle oil temperature, recycle gas flow rate, and quench flow rates. The computation time for the HC unit simulation on a 2.4 GHz Pentium IV computer with 512 MB of SDRAM was about 4 s. The predicted values of bed exit temperatures and product flow rates were compared with the industrial values.

The HC model parameters were fine-tuned using the consistent industrial data. The twelve parameters selected for fine-tuning the model were the amount of heat released per unit consumption of hydrogen, $-\Delta H_{Hcon}$ in kcal/kmol, the frequency factor in the reaction rate constant corresponding to the four catalyst beds in the HC reactor (A_1-A_4 in eq 2), parameters for relative reaction rate kinetics (D_1-D_4 in eq 3), and the product distribution parameters (C, ω, and B) in eqs 4 and 5. The fine-tuning of the 12 parameters was based on minimization of the root of sum of the squared error between the model predictions and the measured values in the plant. The overall objective consisted of the minimization of error in product flow rates, the total of all product flow rates, and the exit temperature from the four catalyst beds.

Objective = Minimize

$$\left(\sqrt{ w_1 \sum_{k=1}^{8}\left(1 - \frac{f_{k,S}}{f_{k,I}}\right)^2 + w_2\left(1 - \frac{F_{T,S}}{F_{T,I}}\right)^2 + w_3 \sum_{i=1}^{4}\left(1 - \frac{T_{outi,S}}{T_{outi,I}}\right)^2 } \right)$$

(9)

Here, w_i (for $i = 1-3$) is the weightage given to each term; here, $w_1 = w_2 = 1$ and $w_3 = 1000$. The 1st term in eq 9 denotes the sum of the squared error between industrial product flow rates ($f_{k,I}$) and the simulated values ($f_{k,S}$) where $k = 1-8$ stands for flow rates of LE, LN, HN, KS, LD, HD, and UCO$_P$ and URO. $F_{T,S}$ and $F_{T,I}$ are the simulated and industrial values of the total sum of these eight flowrates. The 3rd term in eq 9 is the sum of the squared error for outlet bed temperatures between industrial ($T_{outi,I}$) and model predicted values ($T_{outi,S}$). The temperature term is given higher weightage as it is very important to match the temperature of each of the four catalyst beds.

A genetic algorithm[4] (GA) was used for minimizing eq 9 to determine the optimal values of the 12 model parameters (Table 5), using the average data of day 2. The reasons for choosing a GA for fine-tuning the model parameters are several. First, a GA is good at identifying a promising region through global exploration search and it can locate a global optimum in a single run. Direct/stochastic methods such as a GA do not need additional assumptions for optimization problems and are particularly suited for problems with ill- or unknown structures.[39] Though the small number of decision variables suggests the use of a deterministic approach, our experience with the solution of complex nonlinear problems arising from detailed first principle models shows that deterministic methods may fail. This may be because of the difficulty in calculating derivatives
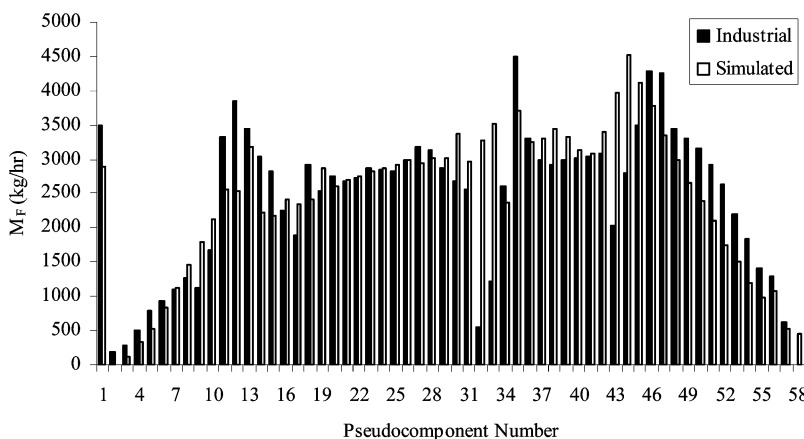
Figure 3. Comparison of model predicted and industrial values of pseudocomponent flow rates.

Table 6. Percentage Error between Industrial Data and Predictions by the HC Unit Model Fine-tuned Using Average Data of Day 2

	% Error = [((Industrial − Prediction) × 100)/Industrial]			
quantity	day 1	day 2[a]	day 3	day 4	day 5
LE	13.67	−13.16 (5.43)	5.75	4.04	17.22
LN	5.35	−4.24 (−34.46)	3.71	−0.18	6.08
HN	12.88	6.08 (−45.24)	10.86	11.94	14.62
KS	−1.58	−1.38 (−3.45)	−1.59	−0.77	−0.34
LD	1.24	2.90 (−1.69)	1.61	2.28	0.79
HD	−30.61	−18.93 (32.39)	−28.23	−28.12	−31.22
UCO$_T$	12.03	27.42 (36.69)	15.16	13.06	5.52
UCO$_P$	−2.64	11.14 (23.67)	2.27	8.87	−0.23
H$_{2,makeup}$	19.98	11.0 (10.9)	16.45	14.73	21.69

[a] The values in parenthesis are the percentage errors in the predictions using the model parameter values reported by Mohanty et al.[13]

of the objective function, which itself involves numerous calculations including numerical solutions of differential equations. Hence, we have employed a GA for fine-tuning as well as optimization of the HC unit.

The optimal values of parameters (Table 5) are comparable to the reported values except for the large differences in −ΔH_{Hcon}, C, and ω. In the present work, the feed is hydrogenated in the HT before its hydrocracking in the HC, whereas the HT was absent in the HC unit simulated in the previous work.[13] Hence, hydrogenation in the present HC and consequently −ΔH_{Hcon} are expected to be less. The optimal values of C and ω together define the production of light ends. If one increases, the other decreases to counterbalance its effect. The reaction rate constants are dependent on the type of feed, shape

and size of the catalyst, and past history of catalyst deactivation. Hence, A_1−A_4 are expected to vary from one bed to another. The predicted temperature profile for day 2's operation is consistent for exothermic reactions and matches with the measured bed exit temperatures (Figure 2). The profiles for beds 3 and 4 show two segments. The probable reason for this is the two types of catalyst (with different densities which affect the rate constant in eq 2) in these two beds. The pseudocomponent flow rates predicted by the model are similar to those calculated from the measured product flow rates on day 2 (Figure 3).

The effect of tuning the model parameters can be seen from the percentage error between the industrial data and the predicted values for product flow rates and H$_{2,makeup}$ for day 2 operation in Table 6. Fine-tuning reduces the average absolute percentage error in these predictions from 22% to 11%. Hence, fine-tuning of the model parameters is essential for good predictions. Predictions could further be improved by fine-tuning activation energies also. However, this was not attempted for two reasons: the activation energy and the frequency factor (pre-exponential factor) are correlated and to avoid too many parameters for tuning.

The model with the optimal values of parameters was used to simulate the HC unit operation for several other days over a period of 3 months. The percentage error between the industrial data and the predicted values for product yields and H$_{2,makeup}$ for these of days of operation are compared in Table 6. Overall, the model is good with an average absolute error of 11% in the prediction of product flow rates. The percentage error in H$_{2,makeup}$

Table 7. Sensitivity Analysis−Effect of Different Variables on HC Unit Performance

	F_{HVGO}		F_{RO}		M_{RG}		T_{RG}		T_{RO}		Q_1		Q_2		Q_3	
% change	−5%	5%	−5%	5%	−5%	5%	−2%	2%	−2%	2%	−5%	5%	−5%	5%	−5%	5%
LE	24.28	−25.50	−4.53	4.41	2.56	−2.36	−30.76	36.39	−35.16	26.84	8.01	−7.58	3.82	−3.67	1.44	−1.42
LN	13.69	−15.89	−3.01	2.90	1.68	−1.55	−21.08	23.11	−24.53	17.24	5.23	−5.03	2.51	−2.43	0.95	−0.94
HN	7.74	−10.65	−2.17	2.06	1.19	−1.11	−15.81	15.63	−18.76	11.84	3.68	−3.62	1.78	−1.74	0.67	−0.67
KS	−6.11	3.78	−0.04	−0.03	−0.03	0.03	−1.19	−1.56	−2.53	−0.83	−0.14	0.00	−0.05	0.02	−0.02	0.02
LD	−7.99	6.11	0.28	−0.33	−0.21	0.20	1.17	−3.86	0.12	−2.57	−0.69	0.55	−0.31	0.28	−0.12	0.12
HD	−17.08	19.45	1.98	−1.90	−1.14	1.09	14.85	−14.84	15.77	−11.06	−3.51	3.47	−1.69	1.66	−0.64	0.65
UCO$_T$	−30.99	49.65	5.16	−4.69	−2.81	2.73	46.32	−31.16	52.87	−24.32	−8.41	9.09	−4.14	4.24	−1.60	1.63
URO	−30.99	49.65	−0.10	0.08	−2.81	2.73	46.32	−31.16	52.87	−24.32	−8.41	9.09	−4.14	4.24	−1.60	1.63
UCO$_P$	−30.99	49.65	36.19	−32.82	−2.81	2.73	46.32	−31.16	52.87	−24.32	−8.40	9.09	−4.14	4.24	−1.60	1.63
H$_{2,consumption}$ in HC	2.31	−3.66	−1.23	1.16	0.67	−0.61	−8.69	9.01	−10.66	6.80	2.07	−2.01	1.00	−0.97	0.37	−0.37
T_{inlet}, K	0.23	−0.33	0.00	0.00	0.04	−0.04	−0.60	0.54	−0.74	0.41	0.07	−0.08	0.04	−0.04	0.01	−0.01
H$_2$, m^3/(m^3 feed) to HC	12.73	−13.64	0.03	−0.02	−0.69	0.70	−10.07	8.16	−11.33	6.25	2.08	−2.15	1.01	−1.02	0.39	−0.39
LHSV, 1/h	−11.29	15.79	−0.03	0.02	−0.68	0.66	11.20	−7.54	12.77	−5.89	−2.03	2.20	−1.00	1.03	−0.39	0.39
X_{pass}	8.05	−10.69	−1.42	1.31	0.78	−0.74	−11.51	9.26	−13.27	7.13	2.36	−2.44	1.15	−1.16	0.44	−0.44
$X_{overall}$	1.42	−2.20	−1.80	1.69	0.15	−0.14	−2.39	1.62	−2.80	1.27	0.43	−0.47	0.21	−0.22	0.08	−0.08
H$_{2,makeup}$	0.57	−0.90	−0.30	0.29	−0.57	0.56	−2.15	2.22	−2.64	1.68	−1.39	1.40	−1.30	1.30	−1.26	1.26

Table 8. Multi-objective Optimization Problems Solved in This Study

problem No.	objective function[a]	decision variables	constraints	fixed variables
case 1	max KS*	$7000 \leq M_{RG}$ (kg/h) ≤ 9000	$T_{inlet} \leq 680$ K	$P_{inlet,HT} = 177$ atm
	min $H^*_{2,makeup}$	$95 \leq F_{HVGO}$ (kL/h) ≤ 115	$T_{out,1} \leq 686$ K	$P_{inlet,HC} = 170$ atm
case 2	max HD*	$630 \leq T_{RG}$ (K) ≤ 680	$T_{out,2} \leq 685$ K	$T_{inlet,HT} = 642$ K
	min $H^*_{2,makeup}$	$610 \leq T_{RO}$ (K) ≤ 655	$T_{out,3} \leq 684$ K	RG1= kg/h[b]
case 3	max HE*	$0.70 \leq F_{RO}$ (−) ≤ 0.92	$T_{out,4} \leq 684$ K	$Q_{HT} =$ kg/h[b]
	min LE*	$1400 \leq Q_1$ (kg/h) ≤ 2200	$0.5 \leq$ LHSV (1/h) ≤ 2.0	purity of $H_{2,Makeup} = 98\%$
		$1400 \leq Q_2$ (kg/h) ≤ 2200	$85 \leq X_{overall}$ (%) ≤ 98	$T_{quench} = 335$ K
		$1200 \leq Q_3$ (kg/h) ≤ 1900	$65 \leq X_{pass}$ (%) ≤ 80	$T_{effluent,HT} = 689$ K

[a] The * symbol indicates that the value is normalized with respect to simulated values for the industrial operation. [b] Value not given due to proprietary reason.

estimate for 5 days of industrial operation is in the range 11−22%. The hydrogen losses in the downstream separation (i.e., with Off-gas1 and Off-gas2) for any day's simulation are fixed at their industrial value. For example, for day 2, it is fixed at 4.2% of the $H_{2,makeup}$. Some amount of hydrogen also gets lost with other gases to flare from distillation column 2 (not shown in Figure 1) and in the wash water separator. Hydrogen has a high solubility in the hydrocarbon mixture at high pressure in the reactor, and it transfers to the gas phase during fractionation at low pressure in the distillation column. Hydrogen is also soluble in the liquid used for wash water separation. Such losses are not measured in industry and, hence, are not considered for simulation. These contribute to the error in the estimate of $H_{2,makeup}$.

Sensitivity Analysis

To formulate the multi-objective optimization problem appropriately, sensitivity analysis was performed by varying one variable at a time around a reference set of values and noting its effect on several performance indicators of the HC unit. The calibrated model was used for sensitivity analysis and was later interfaced with real-coded NSGA-II[40] for plantwide multi-objective optimization. The sensitivity analysis results are summarized in Table 7. The increase in the feed flow rate (F_{HVGO}) increases the production of heavier products (KS, LD, and HD) and unconverted oil (UCO) and decreases the production of lighter products (LE, LN, and HN), as a result of a decrease in the operating temperature and residence time in the reactor. The liquid hourly space velocity (LHSV) increases, thereby decreasing the conversion per pass (X_{pass}) by ∼10% and overall conversion ($X_{overall}$) by ∼2%. The increase in F_{HVGO} has a counter effect on the inlet temperature (T_{inlet}) of the HC. Due to increased LHSV and reduced T_{inlet}, and consequently reduced conversion, H_2 consumption in the HC reduces and the need for $H_{2,makeup}$ decreases by 1%. For the hydrocracking of any heavier pseudocomponent, the formation of lighter pseudocomponents consumes more hydrogen than the formation of heavier components as the C/H ratio for lighter hydrocarbons is much less than that for heavier hydrocarbons.

The increase in the fraction of unconverted oil recycled (F_{RO}) to the reactor is equivalent to processing heavier feed in the reactor. The heat of reaction for hydrocracking of heavier feed is more in comparison to that for hydrocracking of lighter feed. Though the inlet temperature (T_{inlet}) to the reactor is comparable with the plant value (Table 7), a higher operating temperature in the catalyst beds is expected because of the higher exothermic heat of reaction of the heavier feed being processed in the reactor. Hence, both X_{pass} and $X_{overall}$ increase due to the increase in the recycle oil flow rate and the increase in bed temperatures. The overall effect of the increase in LHSV, X_{pass}, and $X_{overall}$ increases the requirement for hydrogen supply to the HC for reaction as well as for quenching.

Table 9. Values of NSGA Parameters for Multi-objective Optimization Studies

NSGA-II parameter	value/specification
number of generations	200
population size	50
encoding technique	real coding
crossover probability	0.85
distribution index for real-coded crossover	10
mutation probability	0.05
distribution index for real-coded mutation	20
seed for random number generator	0.857
crossover parameter in the SBX operator	10.0
variable bounds	rigid
selection strategy	tournament selection

The increase in the mass flow rate of the recycle gas (M_{RG}), RG2 in Figure 1, increases the amount of gas fed to the reactor/m³ of liquid feed. This ultimately decreases T_{inlet} and the bed temperatures, decreasing X_{pass} and $X_{overall}$. The need for $H_{2,makeup}$ goes high due to the increase in the gas flow rate in the process loop. The yield of heavier products can be improved slightly by increasing the recycle gas flow to the HC at the expense of increased cost for recycle gas compression and an increased hydrogen requirement in the process loop. The increase in T_{inlet}, as a result of the increase in recycle gas temperature (T_{RG}) or the recycle oil temperature (T_{RO}), increases the rates of all hydrocracking reactions leading to increase in the production of lighter products such as LE, LPG, LN, and HN but decreases the production of heavier products such as KS, LD, and HD. This ultimately increases the amount of hydrogen required for chemical consumption and for temperature control in the reactor beds by increasing the quench flow rates. The hydrocracking reaction is relatively more sensitive to T_{RG} than to T_{RO} as given by the increase in conversion to 9% and 7% for a 2% increase in each of these temperatures.

Quenching requires a good amount of H_2, and an increase of the quench flow rate (Q_1-Q_3) has a countereffect on temperature. The increase in $H_{2,makeup}$ is expected due to the increased quench flow rate, which also increases the overall gas flow rate to the HC. The increased quench ultimately leads to reduced reaction rates, lower yields of light products, and lower hydrogen consumption for hydrocracking, which is directly related to fractional yield of lighter products.

Multi-objective Optimization

The real life optimization problems faced in industries usually deal with more than one competing objective.[3] Traditionally, solving such problems involves taking a weighted average of all objectives and treating it as a single objective optimization problem. However, the solution then depends on the chosen weights, which in turn are subject to individual perception and knowledge on the process. This is arbitrary, and a deficiency is inherent in the method.[4] The best way to solve and represent the solution of a multi-objective optimization problem is through
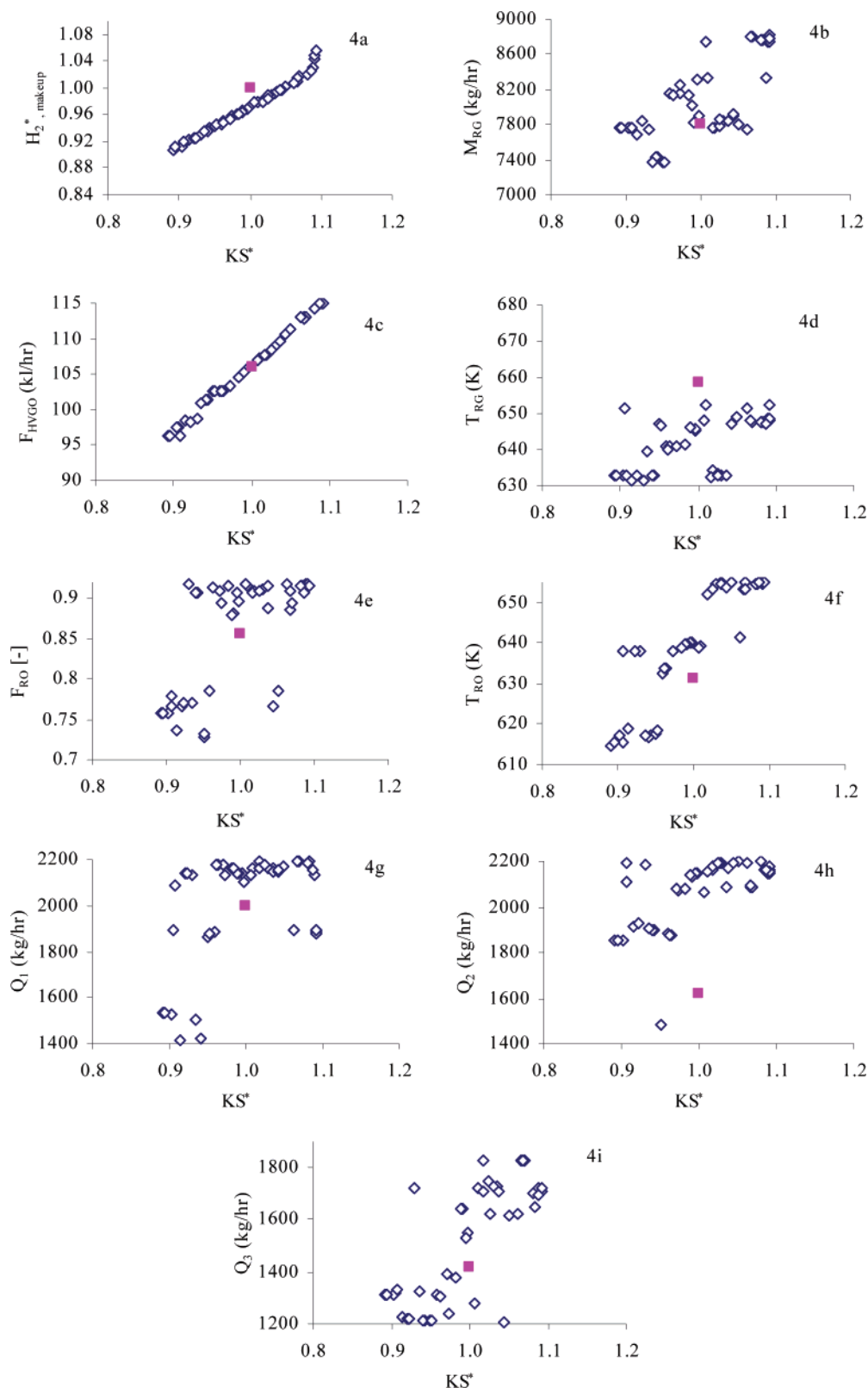
Figure 4. Results for two-objective optimization: the maximization of kerosene and minimization of the makeup H_2 flow rate. (a) Plot of Pareto optimal solutions set. Plots of decision variables corresponding to Pareto optimal solution set in part a are shown in Figure 4b—i: (b) recycle gas flow to hydrocracker; (c) fresh feed flow rate; (d) recycle gas temperature; (e) unconverted recycle oil fraction; (f) unconverted recycle oil temperature; (g) quench flow between bed 1 and 2 in the HC; (h) quench flow between bed 2 and 3 in the HC; (i) quench flow between bed 3 and 4 in the HC. The industrial operating point is shown by the filled square symbol.

generating a Pareto optimal set,[2] which provides a spectrum of tradeoffs of the competing objectives. A Pareto set, for example, for a two objective function problem is described by a set of points such that when one moves from one point to any other,

one objective function improves while the other worsens. All the solutions in a Pareto optimal set are equally good, i.e., none of them is better than the others in the set unless another criterion is supplied to compare them. A Pareto optimal set provides a
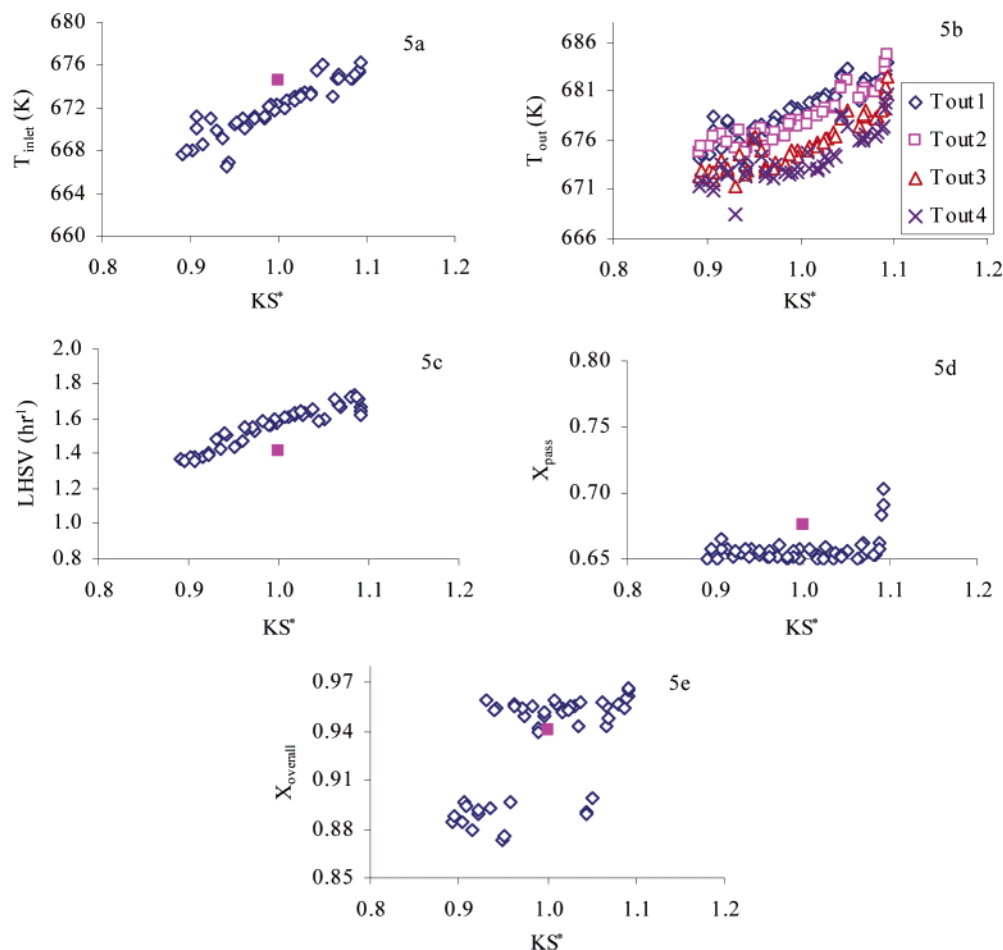
Figure 5. Plot of constraints corresponding to the optimal solution in Figure 4a: (a) inlet temperature to the HC; (b) outlet bed temperatures; (c) LHSV; (d) conversion per pass; (e) overall conversion. The industrial operating point is shown by the filled square symbol.

wide range of design and operational options to designers and practitioners and, hence, enhances the possibility of finding more efficient processes.

In industrial practice, maximization of kerosene, diesel, and naphtha and minimization of off-gases, LPG, and H_2 consumption are the major concerns. Hence, a compromise is often needed between valuable product yield and H_2 consumption. In this work, we have considered three sets of multi-objective problems summarized in Table 8. All the objective functions are normalized using simulated values for the industrial operation (for example, HD* was defined as HD/HD$_{IS}$). Note that, because predictions do not match measured values exactly, simulated (and not actual) values for the industrial operation are used for a fair comparison with the optimal values.

In case 1, the simultaneous maximization of KS and minimization of $H_{2,makeup}$ using eight decision variables is considered. The decision variables are the flow rate of feed (F_{HVGO}), recycle gas mass flow rate (M_{RG}) and temperature (T_{RG}), recycle oil temperature (T_{RO}), recycle oil mass fraction (F_{RO}), which is defined as the ratio of URO to UCO$_T$, and quench flow rates to the catalyst beds, Q_1, Q_2, and Q_3 in Figure 1. Bounds on decision variables given in Table 8 are primarily decided based on possible variation from the current operation and sensitivity analysis. Several constraints are used in the optimization problem formulation. Temperature constraints are important for stable operation of the reactor; constraints for maximum allowable inlet and exit bed temperatures for the HC are also included in Table 8. Apart from the temperature constraints, it is also required to operate the reactor under the trickle flow regime. LHSV (i.e., the flow rate of liquid feed

per unit volume of catalyst) is determined by the residence time requirement based on feed characteristics. The LHSV for the industrial HC is at ca. 1.44 h^{-1}. The X_{pass} and $X_{overall}$ at industrial operating conditions lie between 65% and 75% and 93% and 97.5%, respectively. The $X_{overall}$ and X_{pass} should be maintained within these limits to accommodate the feed and operating cost for recycle, avoiding overloading the catalyst with heavy feed that contains a high concentration of polyaromatics, which usually are difficult to crack. Fixed variables based on the typical operating conditions in the plant are also presented in Table 8. The T_{inlet} to the HC is evaluated by calculating the enthalpy of three streams: the effluent from the HT, the recycle gas (RG2) and the unconverted recycle oil (URO). For this, the temperature of the HT effluent stream is fixed at the industrial value of 689 K.

In the second case, the maximization of HD and minimization of $H_{2,makeup}$ is studied. Since the cost of HD is competitive with that of KS, its high demand may result in equal returns when compared with the case of KS. In the third case, the maximization of high-value end (HE) products and minimization of low-value end (LE) products is studied. HE is defined as the sum of all products excluding light gases and UCO$_T$ (i.e., LN + HN + KS + LD + HD), whereas LE includes all the light components excluding H_2S and H_2 from off-gases.

Population based algorithms, such as a genetic algorithm (GA), have the capability of finding a Pareto optimal set in a single run with only a marginal increase in the computational time. On the basis of the fundamentals of a GA, Srinivas and Deb[41] developed the *nondominated sorting genetic algorithm* (NSGA), to find Pareto optimal sets of solutions for solving
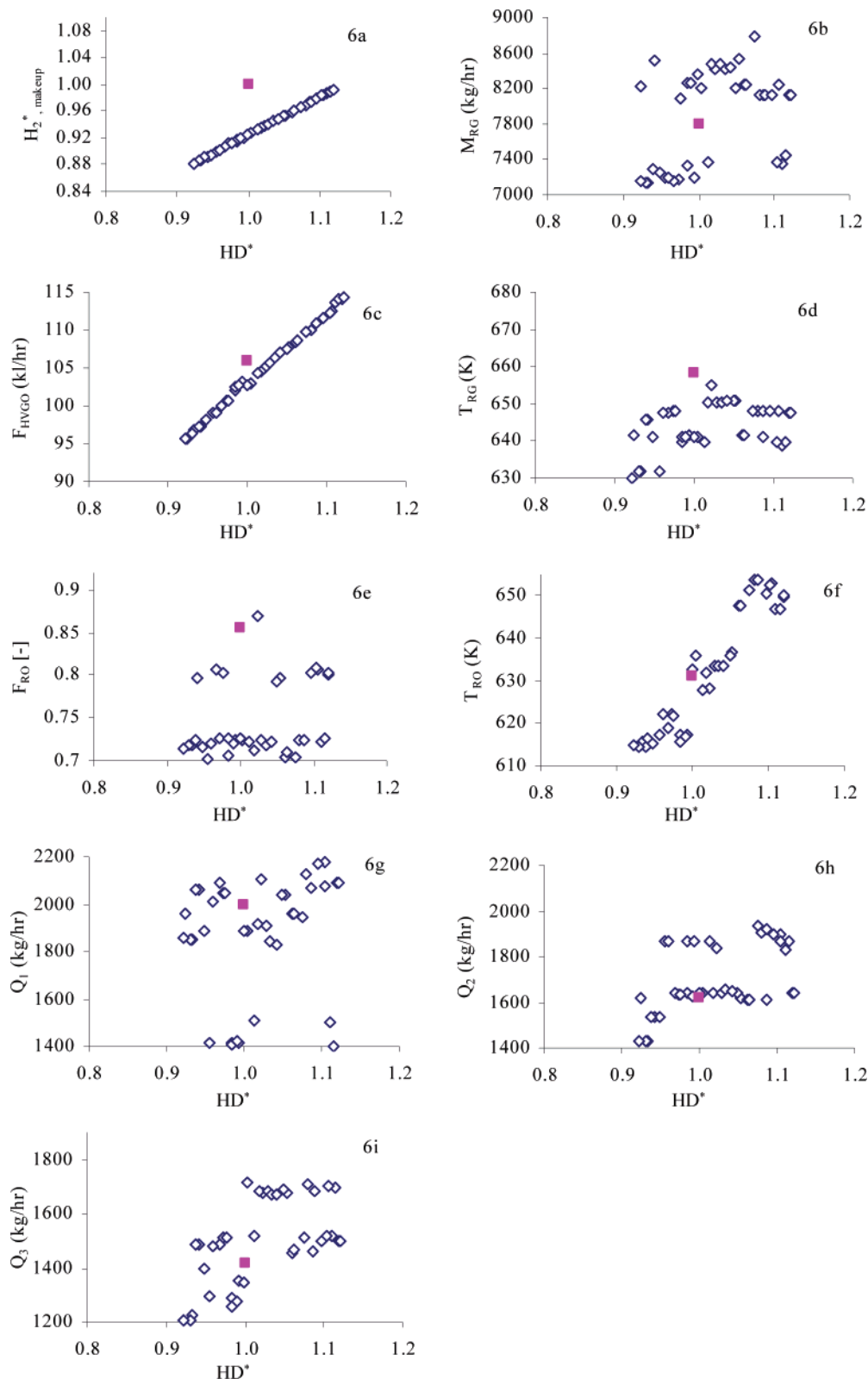
Figure 6. Results for two-objective optimization: the maximization of heavy diesel and minimization of the makeup H_2 flow rate. (a) Plot of Pareto optimal solutions set. Plots of decision variables corresponding to Pareto optimal solution set in part a are shown in Figure 6b−i: (b) recycle gas flow to hydrocracker; (c) fresh feed flow rate; (d) recycle gas temperature; (e) unconverted recycle oil fraction; (f) unconverted recycle oil temperature; (g) quench flow between bed 1 and 2 in the HC; (h) quench flow between bed 2 and 3 in the HC; (i) quench flow between bed 3 and 4 in the HC. The industrial operating point is shown by the filled square symbol.

multi-objective optimization problems. Although NSGA was successfully applied to many multi-objective optimization problems (e.g., Rajesh et al.[42]), Deb et al.[40] reported that its computational complexity can be drastically reduced and, by applying elitism (a method of preserving good solutions), its

performance can be further improved. This modification in NSGA resulted in *elitist* NSGA (or NSGA-II). They[40] have shown that NSGA-II is able to achieve better convergence to the true Pareto optimal front and to find a better spread of Pareto optimal solutions.
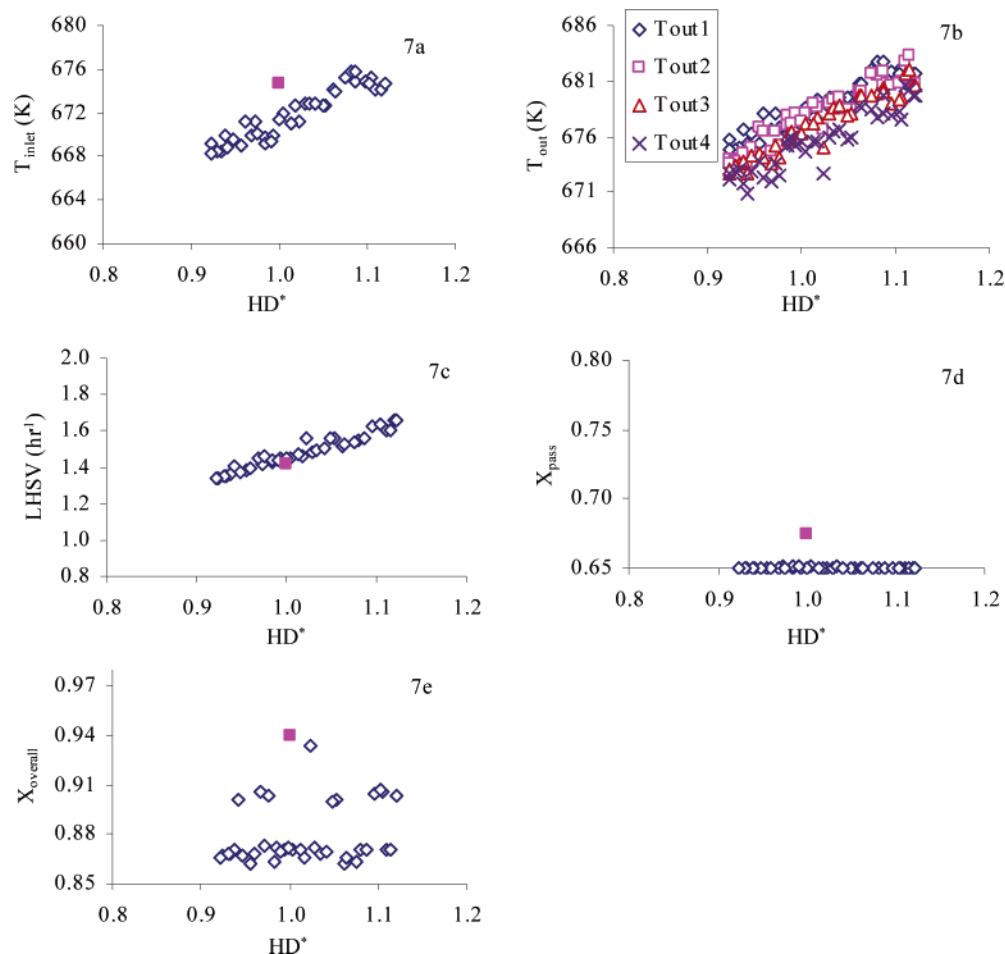
Figure 7. Plot of constraints corresponding to optimal solution in Figure 6a: (a) inlet temperature to the HC; (b) outlet bed temperatures; (c) LHSV; (d) conversion per pass; (e) overall conversion. The industrial operating point is shown by the filled square symbol.

GA operators, designed to be applied in binary numbers, need binary coding for the real values of decision variables. However, it was noted[40] that representing real numbers with binary coding leads to a number of difficulties such as the fact that finite-length binary strings are unable to achieve high precision in the decision variables. Moreover, transition to a neighboring point requires the alteration of many bits which in turn hinders the gradual search in the continuous search space (known as the Hamming cliff problem). To counter these problems, genetic operators, capable of operating directly on real numbers, have been proposed. The simulated binary crossover (SBX) operator, proposed by Deb and Agrawal,[43] is a very successful example. In our earlier studies,[44] we noted that the SBX operator, which mimics the operation of binary crossover, is able to perform as good as or even better than the binary coded GAs. The present study employs real-coded NSGA-II with a SBX operator. The computational parameters used in this study are given in Table 9. All the optimization studies were carried out with a population size of 50 for 200 generations. The average computational time for obtaining a Pareto optimal set was ca. 16 h on a 2.4 GHz Pentium 4 computer with 512 MB of SDRAM.

Results and Discussion

Figure 4 shows the results for case 1: the simultaneous maximization of KS* and minimization of $H^*_{2,makeup}$. KS* is relatively more expensive, and its maximization will generate more revenue. The optimal Pareto obtained (in Figure 4a) shows a contradictory behavior between the two objectives, i.e., when
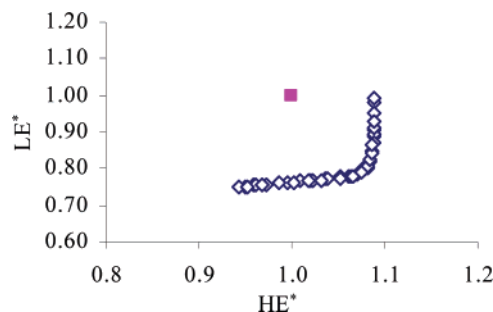

Figure 8. Pareto optimal solution for two-objective optimization: the maximization of heavy-end products (HE) and minimization of light-end products (LE). The industrial operating point is shown by the filled square symbol.

KS* increases, $H^*_{2,makeup}$ also increases. Many optimal solutions with $H^*_{2,makeup}$ in the range 0.9–1.06 and KS* in the range 0.9–1.0 are available for selection by the decision maker for industrial operation. Figure 4 also shows the potential for enhancing the current industrial operation.

The plots for decision variables corresponding to the optimal Pareto are also shown in Figure 4b–i, while the plots for the constraints are shown in Figure 5. KS* increases with both F_{HVGO} (Figure 4c) and T_{inlet} (Figure 5a). LHSV, which is directly related with total liquid feed to the reactor, increases with both F_{RO} (Figure 4e) and F_{HVGO} (Figure 5c). Hence, the reactor temperature shall increase with an increase in LHSV in order to maintain X_{pass} within allocated bounds, which hits the lower bound (Figure 5d). The inlet temperature increase is a result of
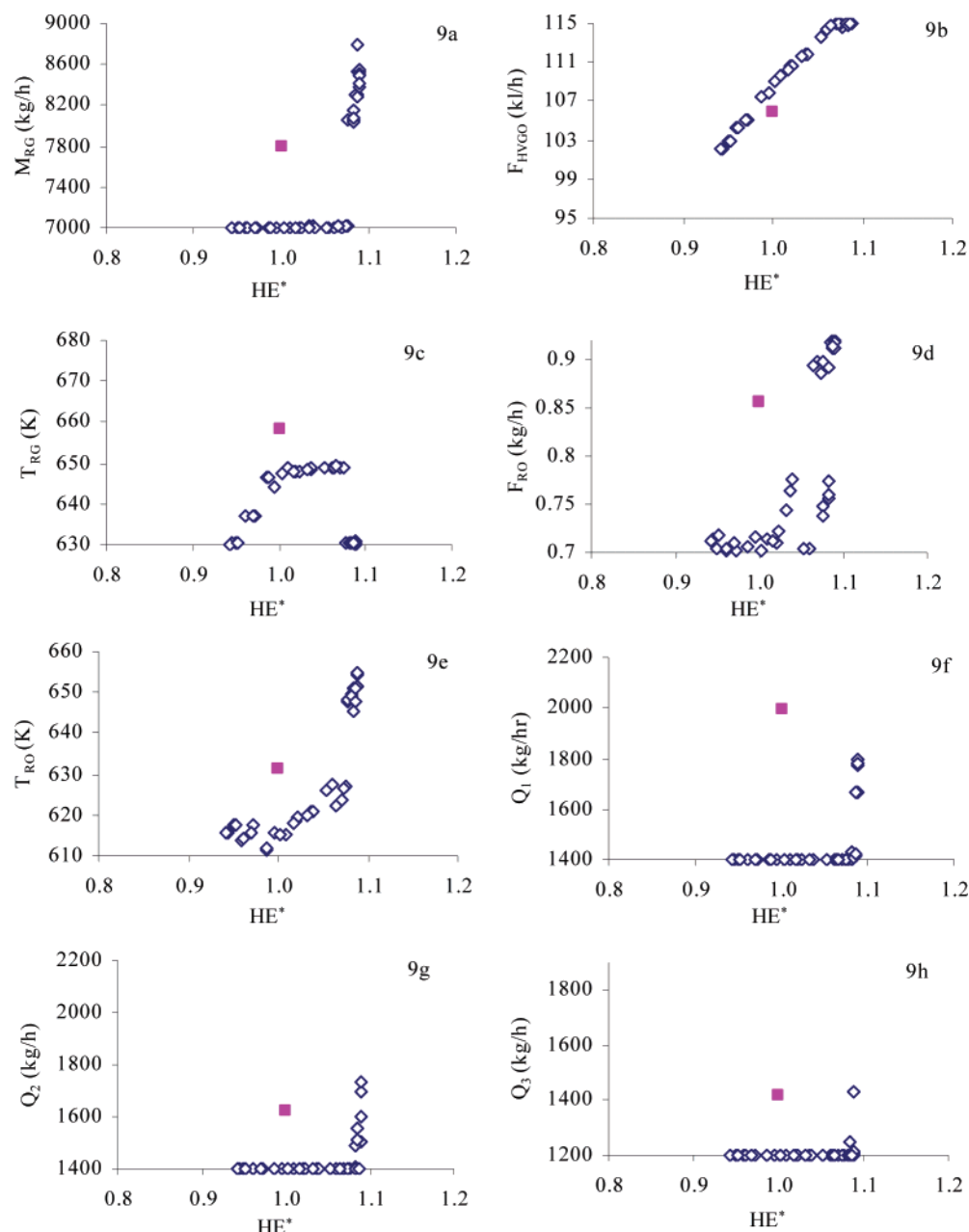
Figure 9. Plots of decision variables corresponding to Pareto optimal solution in Figure 8: (a) recycle gas flow to hydrocracker; (b) fresh feed flow rate; (c) recycle gas temperature; (d) unconverted recycle oil fraction; (e) unconverted recycle oil temperature; (f) quench flow between bed 1 and 2 in the HC; (g) quench flow between bed 2 and 3 in the HC; (h) quench flow between bed 3 and 4 in the HC. The industrial operating point is shown by the filled square symbol.

the increase in T_{RG} (Figure 4d) and T_{RO} (Figure 4f) and of the corresponding increase in the enthalpy of the feed with an increase in the feed flow rate and M_{RG}. More recycle gas at the HC inlet (Figure 4b) is required to saturate the liquid feed as the production of heavier product is favored at a higher degree of saturation and lower temperature. As a result of the increase in the operating inlet temperature and bed temperatures with the increase in the flow rate of the feed, the cooling requirement also increases. The intermediate quench rates (Figure 4g−i) depend on the cooling requirement. The fraction of unconverted oil recycled, F_{RO} (Figure 4e), is found to have a direct relation to $X_{overall}$ (Figure 5e). The value of X_{pass} (Figure 5d) is lower in comparison to the plant operating value of 0.675 and remains constant at 0.65 until F_{HVGO} is close to its upper bound. At this point, one of the ways to increase the production rate of KS* is to increase X_{pass} by cooling less between the beds, as indicated

by Q_1 and Q_3 dropping at high values of KS* (Figure 4g and h). But, the expected gain in X_{pass} and the related increase in KS* are limited as the production of KS* is favored at lower values of X_{pass}. This, however, needs more hydrogen for reaction and, subsequently, more $H^*_{2,makeup}$, as can be seen by the sudden increase at high values of KS* in Figure 4a. The increase in outlet bed temperatures (Figure 5b) also corresponds to an increase in T_{inlet}.

The results for case 2 are shown in Figure 6: the simultaneous maximization of HD* and minimization of $H^*_{2,makeup}$. Like KS*, HD* is sold at competitive prices and has good demand. Similar to case 1, the optimal Pareto obtained (Figure 6a) shows a contradictory behavior between the two objectives: when HD* increases, $H^*_{2,makeup}$ also increases. It also offers many optimal solutions to the decision maker. Figure 6a shows that current
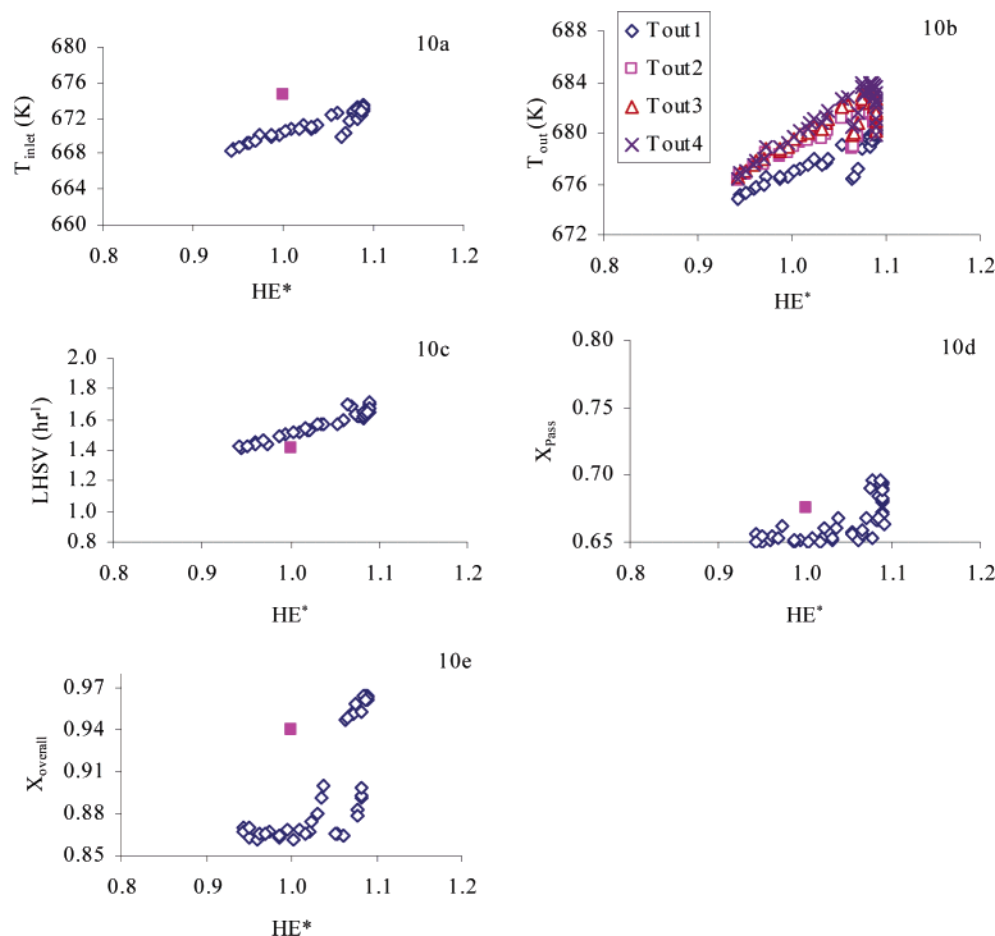
Figure 10. Plot of constraints corresponding to optimal solution in Figure 8: (a) inlet temperature to the HC; (b) outlet bed temperatures; (c) LHSV; (d) conversion per pass; (e) overall conversion. The industrial operating point is shown by the filled square symbol.

industrial operation can be improved to increase HD* by ~10% without increasing $H^*_{2,makeup}$ or to decrease $H^*_{2,makeup}$ by ~8% without changing HD*. The effect of fixing F_{HVGO} in case 2 is discussed in the Appendix.

The plots for the decision variables corresponding to the objective function are also shown in Figure 6b–i, while the plots for the constraints are shown in Figure 7. The trends in operating decision variables, M_{RG}, F_{HVGO}, T_{RG}, and T_{RO} (Figure 6b–d and f), are quite similar to case 1, but the overall effect of a decrease in M_{RG}, T_{RG}, and T_{RO} in the latter part is a slight drop in T_{inlet} (Figure 7a). Though objective space has converged to a Pareto with good spread, the variable space of M_{RG}, F_{RO}, T_{RG}, and T_{RO} is quite scattered. Multiple optimal solutions are possible, and hence, variables such as T_{RG} (Figure 6d) converge to two parallel trends. Similarly, optimal Q_2 and Q_3 show some trend, while Q_1 is scattered around the industrial value. The quench flow rates (Q_1, Q_2, and Q_3), shown in Figure 6g–i, normally increase with an increase in the cooling requirement to extract the heat of hydrocracking. There are two ways to increase HD*: by increasing F_{RO} and operating the reactor at a relatively lower temperature and by increasing F_{HVGO} and T_{inlet} simultaneously while keeping F_{RO} constant at a lower value. HD* increases with the increase in T_{inlet} (Figure 7a) and F_{HVGO} (Figure 6c). F_{RO} converges around two optimal values 0.8 and 0.7. The higher values of F_{RO} (in Figure 6e) chosen by the optimizer correspond to relatively lower inlet and outlet bed temperatures in Figure 7a and b. $X_{overall}$ is directly related to F_{RO} as in the previous case, while X_{pass} maintains a constant value of 0.65 throughout (Figure 7d and e).

Refiners often encounter limited availability of $H_{2,makeup}$ from the naphtha reforming unit and/or limited HVGO feed, which may lead to a shutdown of the HC unit or the need to operate the plant at lower throughput. If a timely decision is made to operate the unit at its optimum with a lower feed flow rate and/ or increased overall conversion by increasing the recycle, the shutdown can be delayed. Hence, the range of solutions of the above-mentioned optimization problems (cases 1 and 2) is useful to industry when a limited amount of hydrogen is available from the upstream reformer unit, and the best utilization of feed and maximization of KS or HD are the main objectives.

The Pareto optimal solution obtained for case 3 is shown in Figure 8 where heavier end (HE*) products is maximized while minimizing light-end (LE*) products. The overall effect is a result of a combination of optimal decision variable sets chosen by the optimizer. Figures 9 and 10 show the corresponding values for decision variables and constraints. Figure 9 shows that a 9% increase in HE or a 25% decrease in LE* is possible when compared to their simulated values for industrial operation. The increase in F_{HVGO} has a counter effect on the residence time of liquid in the reactor, thereby reducing conversion. Hence, the HC inlet temperature needs to be increased (Figure 10a) with the increase in F_{HVGO} to maintain conversion within plant operating limits (Figure 10d and e). The rise in T_{inlet} (Figure 10a) is governed by the increase in T_{RO} (Figure 9e) and T_{RG} (Figure 9c). As shown in Table 7, a 2% increase in T_{RG} (keeping all other variables constant at plant operating values) increases LE production by 36% and decreases HD production by 14.8%; on the other hand, a 2% increase in T_{RO} increases LE by 26.8%
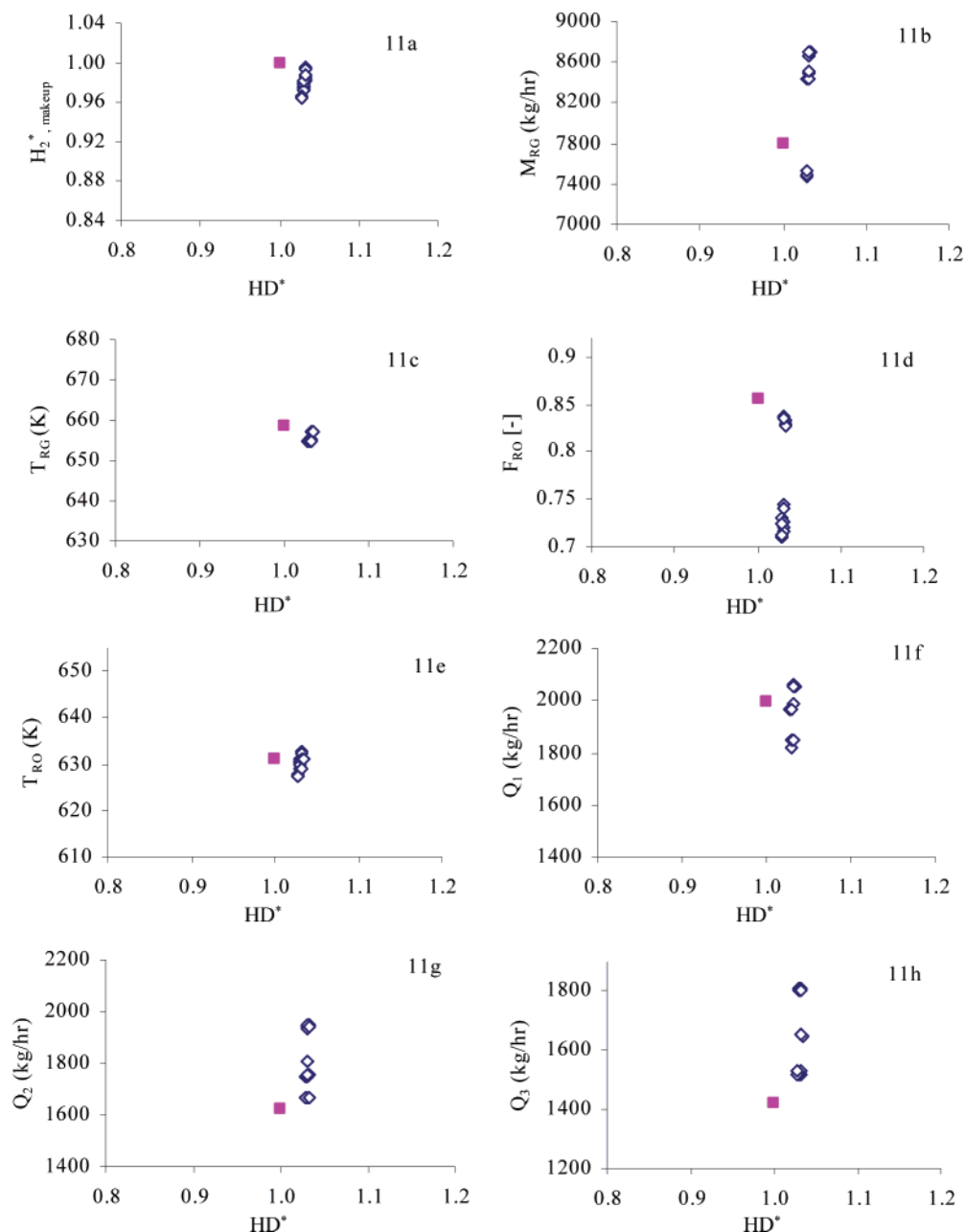
Figure 11. Results for two-objective optimization: the maximization of heavy diesel and minimization of the makeup H_2 flow rate. (a) Plot of Pareto optimal solutions set. Plots of decision variables corresponding to Pareto optimal solution set in part a are shown in Figure 11b−i: (b) recycle gas flow to hydrocracker; (c) recycle gas temperature; (d) unconverted recycle oil fraction; (e) unconverted recycle oil temperature; (f) quench flow between bed 1 and 2 in the reactor; (g) quench flow between bed 2 and 3 in the reactor; (h) quench flow between bed 3 and 4 in the reactor. The industrial operating point is shown by the filled square symbol.

and decreases HD by 11%. Hence, T_{inlet} needs to be kept under control and should vary optimally with increases in F_{HVGO} in order to limit X_{pass} and have a lesser amount of LE in the product.

When the feed flow rate hits its upper bound, one way to increase HE is through increase in the URO flow and, so, the recycle oil fraction shoots to a high value (Figure 9d). The overall effect of the increase in the recycle gas flow, recycle oil flow, and recycle oil temperature is the increase in the inlet reactor temperature and X_{pass} and, ultimately, $X_{overall}$ (Figure 10d to e). To counteract the exit temperature from bed 1, Q_1, Q_2, and Q_3 try to attain a higher value (Figure 9f−h). This can be explained by the effect of Q_1, Q_2, and Q_3 on production of light ends, which can be reduced by 7.6% with a 5% increase in Q_1, whereas a similar increase in Q_2 and Q_3 results in only 3.7% and 1.42% decrease, respectively (Table 7).

The temperature control in the HC is very important to avoid reaction runaway. The inlet and outlet bed temperatures are within the specified limits (Figure 10a and b). The liquid hourly velocity is slightly higher than that for the plant operating conditions (Figure 10c) and increases with the increase in the feed flow rate except for the slight drop for some points at high values of HE in the later part, which is most likely due to a drop in unconverted recycle oil (Figure 9d). These points are followed by an increase in LHSV due to the increase in F_{RO} at the constant value achieved by F_{HVGO} when it hits its upper bound (Figure 9b).

In all the case studies, the X_{pass} is found to be close to its lower bound, which is less as compared to the industrial operating value and increases (for case 1 and case 3, as shown in Figures 5d and 10d) when F_{HVGO} reaches its upper bound (Figures 4c and 9b). This suggests that X_{pass} shall be kept low
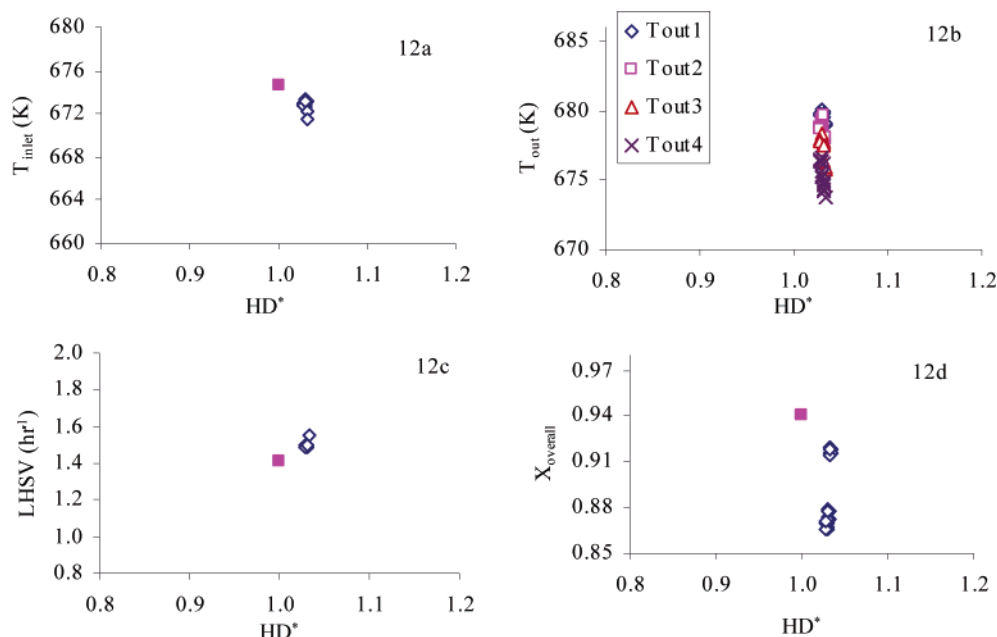
Figure 12. Plot of constraints corresponding to optimal solution in Figure 11a: (a) inlet temperature to the HC; (b) outlet bed temperatures; (c) LHSV; (d) overall conversion. The industrial operating point is shown by the filled square symbol.

to increase HD and KS as well as HE. In case 1, the URO would increase as a result of a decrease in X_{pass} (Figure 5d) and an increase in F_{RO} (Figure 4e), whereas, in case 2, the decrease in X_{pass} (Figure 7d) together with $X_{overall}$ (Figure 7e) suggests an increase in UCO_T. A similar effect of these variables are seen in case 3. The decrease in X_{pass} increases the cost for pumping URO and heating it in shell and tube heat exchangers. The operating cost which basically comprises energy consumption in fired heaters, pumping, and compression is not known from the industry. With the availability of more information from the plant, the work could be extended toward a three objectives problem with an operating cost function as one of the objectives to find a host of other useful solutions and to make a quantitative estimate of the operating cost with respect to variable operating scenarios.

Conclusions

A kinetic model based on the discrete lumped approach was implemented for simulation of an industrial HC unit. The feed and products were characterized by 58 pseudocomponents using available experimental/industrial data and Hysys. The mass fractions of the pseudocomponents in the feed and products were also estimated. The kinetic and product distribution parameters in the HC model were then fine-tuned using daily average operating data from the industry. The model can reasonably predict the flow rates of various products, the hydrogen consumption, the makeup hydrogen requirement, and the temperature profile in the HC.

Multi-objective optimization of the industrial HC unit for three cases of two objectives was performed using real-coded *elitist* NSGA. These optimization problems included several decision variables and constraints based on industrial practice. The study reveals a wide range of options for optimal operation. The improvements in the production of kerosene, heavy diesel, and heavy-end products and the conservation of makeup H_2 or the lower production of light-ends are quantitatively described. The results revealed that reactor performance is most sensitive to operating temperature and that inclusion of feed flow as a decision variable could bring further improvements. Refiners

often face problems due to a shortage of HVGO feed and/or makeup hydrogen. Since the feed flow rate has a direct effect on the production rate and is an important variable to step-up or step-down the production, the present study and its results are useful for finding optimal values of decision variables to maximize production of desired products while minimizing undesired products or hydrogen consumption.

Appendix

An additional problem of case 2 (the maximization of HD^* and minimization of $H^*_{2,makeup}$) with seven decision variables, by fixing F_{HVGO} at its industrial value, has also been considered to examine the window of operation and expected benefits. The results (Figure 11a) show that though it is possible to increase HD^* by ~3% and reduce $H^*_{2,makeup}$ by 4%, the range of optimal solutions is limited. The decision variables, T_{RG} (Figure 11c) and T_{RO} (Figure 11e), converge around single points, whereas M_{RG}, F_{RO}, Q_1, Q_2, and Q_3 (Figure 11b, d, and 11f−h) show a good spread. It is therefore possible to increase HD^*, but there needs to be an increase in M_{RG} (Figure 11b) and F_{RO} (Figure 11d) as well as in the quench flow rates (Figure 11f−h). The reactor is operated at a relatively lower T_{inlet} (Figure 12a) and higher LHSV (Figure 12c) in comparison to the actual plant operation, while X_{pass} is maintained at its minimum value of 0.65. Results in Figure 11 compared to those for case 2 in Figure 6 indicate that F_{HVGO} is an important decision variable to give a broad range of optimal solutions.

Nomenclature

A = frequency factor, volume of feed/(volume of catalyst h)
B, C = product distribution parameters, (-)
C_i = mass fraction of pseudocomponent i in the mixture, (-)
C_{pi} = specific heat capacity of pseudocomponent i, kcal/(kg K)
CN = carbon number, (-)
C/H = carbon to hydrogen weight ratio, (-)
D_i = constants for relative rate expression ($i = 1$−4 in eq 5)
E = activation energy, kcal/kmol

FBP = final boiling point, °C

F_{RO} = unconverted oil mass fraction; URO/UCO$_T$, (-)

F_{HVGO} = volumetric flow rate of HVGO, kL/h

$f_{k,I}$ = industrial product and URO flow rate (k = 1−8), kg/h

$f_{k,S}$ = simulated product and URO flow rate (k = 1−8), kg/h

$F_{T,I}$ = sum of industrial products and URO flow rate, kg/h

$F_{T,S}$ = sum of simulated products and URO flow rate, kg/h

HD = heavy diesel mass flow rate, kg/h

HE = heavy ends mass flow rate, kg/h

HVGO = heavy vacuum gas oil

$H_{2,makeup}$ = makeup hydrogen flow rate, kg/h

HC = hydrocracker

HN = heavy naphtha mass flow rate, kg/h

HPS = high-pressure separator

HT = hydrotreater

$HT_{effluent}$ = hydrotreater liquid effluent

IBP = initial boiling point, °C

k_i, k_j = overall first-order reaction rate constant for the cracking of pseudocomponent, kg of reactant/(kg of catalyst h)

K_i = relative reaction rate function

KS = kerosene mass flow, kg/h

LD = light diesel mass flow rate, kg/h

LE = light-ends mass flow rate, kg/h

LHSV = liquid hourly space velocity, 1/h

LN = light naphtha mass flow rate, kg/h

LPG = liquefied petroleum gas flow rate, kg/h

LPS = low-pressure separator

M_i = mass flow rate of pseudocomponent i, kg/h

M_{RG} = mass flow rate of recycle gas to the HC, kg/h

M_t = mass flow rate of feed, kg/h

MW = molecular weight, g/mol

M_{cat} = mass of catalyst, kg

N = number of pseudocomponents

P_{inlet} = inlet pressure to the HC, atm

P'_{ij} = cumulative products yield until pseudocomponent i from hydrocracking of the pseudocomponent j

P_C = critical pressure, atm

Q_{HT} = total quench flow rate to hydrotreater, kg/h

Q_{HC} = total quench flow rate to hydrocracker, kg/h

Q_1, Q_2, Q_3 = quench flow rate between the beds in the hydrocracker, kg/h

RG1 = recycle gas flow rate to the HT, kg/h

RG2 = recycle gas flow rate to the HC, kg/h

R = ideal gas constant, 2.0 cal/(mol K)

R_s = seed for random number generator

T = operating reactor temperature, K

T_{bj} = boiling point of pseudocomponent j, °C

TBP = true boiling point of pseudocomponent, K

T_C = critical temperature, K

T_{inlet} = inlet temperature to the HC, K

$T_{inlet,i}$ = inlet temperature to bed i, K

$T_{out,i}$ = outlet temperature of bed i of the HC, K

T_{RG} = temperature of recycle gas to the HC, K

T_{RO} = temperature of recycle oil to the HC, K

UCO_T = total flow rate of unconverted oil, kg/h

UCO_P = flow rate of unconverted oil product, kg/h

URO = flow rate of unconverted recycle oil, kg/h

Watson K = Watson characterization factor, (-)

V_C = critical volume, cm^3/mol

V_{cat} = volume of catalyst, m^3

w_i = weight for each term in the objective function (i = 1−3 in eq 10)

WWS = wash water separator

W = weight of the catalyst bed, kg

x_{LN} = mass fraction of pseudocomponent in light naphtha, (-)

x_{HN} = mass fraction of pseudocomponent in heavy naphtha, (-)

x_{HVGO} = mass fraction of pseudocomponent in feed (HVGO), (-)

x_{HD} = mass fraction of pseudocomponent in heavy naphtha, (-)

y_{LN} = fractional distribution of pseudocomponent in light naphtha, (-)

y_{HN} = fractional distribution of pseudocomponent in heavy naphtha, (-)

X_{pass} = conversion per pass on product basis in weight fraction (HD + LD + KS + LN + HN + LE)/(HD + LD + KS + LN + HN + LE + UCO$_T$), (-)

$X_{overall}$ = overall conversion on product basis in weight fraction (HD + LD + KS + LN + HN + LE)/(HD + LD + KS + LN + HN + LE + UCO$_P$), (-)

y_{ij} = normalized boiling point of pseudocomponent i to pseudocomponent j, (-)

Z_C = compressibility factor

Greek Symbols

ρ_{HVGO} = feed density, kg/m^3

$\rho_{catalyst}$ = catalyst density, kg/m^3

$-\Delta H_{Hcon}$ = heat of hydrocracking per unit amount of hydrogen consumed, kcal/kmol

$\hat{\phi}_i$ = fugacity coefficient of a pseudocomponent

ω = product distribution parameter and acentric factor

$(-\Delta H°)_{Rj}$ = standard heat of reaction for hydrocracking of pseudocomponent j per unit mass of hydrocarbon reactant, kcal/kg

$(-\Delta H)_{Rj}$ = heat of reaction for hydrocracking of pseudocomponent j per unit mass of hydrocarbon reactant, kcal/kg

Subscripts/Superscripts

i, j = pseudocomponent number

* = normalized using simulated value for the industrial operation

IS = simulated value for industrial operation

Literature Cited

(1) Meyers, R. A. *Handbook of Petroleum Refining Processes*, 2nd ed.; McGraw-Hill: New York, 1996.

(2) Chankong, V.; Haimes, Y. Y. *Multi-objective Decision Making− Theory and Methodology*; Elsevier: New York, 1983.

(3) Bhaskar, V.; Gupta, S. K.; Ray, A. K. Applications of multi-objective optimization in chemical engineering. *Rev. Chem. Eng.* **2000**, *16*, 1.

(4) Deb, K. *Multi-objective optimization using evolutionary algorithms*; Wiley: New York, 2001.

(5) Weekman, V. W.; Nace, D. M. Kinetics of catalytic cracking selectivity in fixed, moving and fluid bed reactors. *AIChE J.* **1970**, *16* (3), 397.

(6) Nandasana, A. D.; Ray, A. K.; Gupta, S. K. Applications of the Nondominated Sorting Genetic Algorithm (NSGA) in Chemical Reaction Engineering. *Int. J. Chem. Reactor Eng.* **2003**, *1* (R2); www.bepress.com/ ijcre/vol1/R2/.

(7) Ali, M. A.; Tasumi, T.; Masuda, T. Development of heavy oil hydrocracking catalyst using amorphous silica−alumina and zeolite as catalyst supports. *Appl. Catal., A* **2002**, *233*, 77.

(8) Al-Dahhan, M. H.; Larachi, F.; Dudukovic, M. P.; Laurent, A. High-pressure trickle-bed reactors: a review. *Ind. Eng. Chem. Res.* **1997**, *36*, 3292.

(9) Stangeland, B. E. A kinetic model for the prediction of hydrocracker yields. *Ind. Eng. Chem. Process Des. Dev.* **1974**, *13* (1), 71.

(10) Quader, S. A.; Hill, G. R. Hydrocracking of gas oils. *Ind. Eng. Chem. Process Des. Dev.* **1969**, *8* (1), 98.

(11) Korre, S. C.; Klien, M. T. Hydrocracking of polyaromatics Hydrocarbons, development of rate through inhibition studies. *Ind. Eng. Chem. Res.* **1997**, *36*, 2041.

(12) Callegas, M. A.; Martinez, M. T. Hydrocracking of a Maya residue: kinetics and products yield distributon. *Ind. Eng. Chem. Res.* **1999**, *38*, 3285.

(13) Mohanty, S.; Saraf, D. N.; Kunzru, D. Modeling of a hydrocracking reactor. *Fuel Process. Technol.* **1991**, *29*, 1.

(14) Baltanas, M. A.; Froment, G. F. Computer generation of reaction networks and calculation of product distributions in the hydroisomerisation and hydrocracking of paraffins on Pt-containing bifunctional catalysts. *Comput. Chem. Eng.* **1985**, *9*, 77.

(15) Schweitzer, J. M.; Glatier, P.; Schweich, D. A single events kinetic model for the hydrocracking of paraffins in a three-phase reactor. *Chem. Eng. Sci.* **1999**, *54*, 2441.

(16) Liguras, D. K.; Allen, D. T. Structural Models for Catalytic Cracking: 1. Model Compounds Reactions. *Ind. Eng. Chem. Res.* **1989**, *28*, 655.

(17) Gray, M. R. Lumped kinetics of structural groups: hydrotreating of heavy distillate. *Ind. Eng. Chem. Res.* **1990**, *29* (4), 505.

(18) Quann, R. J.; Jaffe, S. B. Structureoriented lumping: describing the chemistry of complex hydrocarbon mixtures. *Ind. Eng. Chem. Res.* **1992**, *31*, 2483.

(19) Quann, R. J.; Jaffe, S. B. Building Useful Models of Complex Reaction Systems in Petroleum Refining. *Chem. Eng. Sci.* **1996**, *51*, 1615.

(20) Martens, G. G.; Marin, G. B. Kinetics and hydrocracking based on structural classes: Model development and application. *AIChE J.* **2001**, *47*, 1607.

(21) Martens, G. G.; Thybaut, J. W.; Marin, G. B. Single Event Parameters for Hydrocracking of Cycloalkanes on Pt/US−Y Zeolites. *Ind. Eng. Chem. Res.* **2001**, *40*, 1832.

(22) Ho, T. C.; Aris, R. On Apparent Second-Order Kinetics. *AIChE J.* **1987**, *33*, 1050.

(23) Chou M. Y.; Ho, T. C. Continuum theory for lumping nonlinear reactions. *AIChE J.* **1988**, *34*, 1519.

(24) Aris, R. On reactions in Continuous Mixtures. *AIChE J.* **1989**, *35*, 539.

(25) Astarita, G.; Nigam, A. Lumping nonlinear kinetics in a CSTR. *AIChE J.* **1989**, *35*, 1927.

(26) Chou, M. Y.; Ho, T. C. Lumping coupled nonlinear reactions in continuous mixtures. *AIChE J.* **1989**, *35*, 533.

(27) Cicarelli, P.; Astarita, G.; Gallifuoco, A. Continuous kinetic lumping of catalytic cracking processes. *AIChE J.* **1992**, *38*, 7.

(28) Basak, K.; Sau, M.; Manna, U.; Verma, R. P. Industrial hydrocracker model based on novel continuum lumping approach for optimization in petroleum refinery. *Catal. Today* **2004**, *98* (1−2), 253.

(29) Browarzik, D.; Kehlen, H. Hydrocracking process of *n*-Alkanes by continuous kinetics. *Chem. Eng. Sci.* **1994**, *49*, 923.

(30) Laxminarasimhan, C. S.; Verma, R. P.; Ramachandran, P. A. Continuous lumping model for simulation of hydrocracking. *AIChE J.* **1996**, *42*, 2645.

(31) Pacheco, M. A.; Dassori, C. G. Hydrocracking: An improved kinetic model and reactor modeling. *Chem. Eng. Commun.* **2002**, *189*, 1684.

(32) Wauquier, J. P. *Petroleum Refining*; Editions Technip: Paris, 2000.

(33) Lee, B. I.; Kesler, M. G. A generalized thermodynamic correlation based on three-parameter corresponding states. *AIChE J.* **1975**, *21* (3), 510.

(34) Reid, R. C.; Prausnitz, J. M.; Poling, B. E. *The properties of gases and liquids*; McGraw-Hill: New York, 1987.

(35) Walas, S. H. *Phase Equilibria in Chemical Engineering*; Butterworth Publishers: Markham, OH, Canada, 1985.

(36) Weir, H. M.; Eaton, G. L. *Ind. Eng. Chem.* **1932**, *24*, 211.

(37) Smith, J. M.; Van Ness, H. C. *Introduction to Chemical Engineering Thermodynamics*; McGraw-Hill: New York, 2001.

(38) Nelson, W. L. *Petroleum refinery engineering*, 4th ed.; McGraw-Hill: New York, 1958; p 169.

(39) Pardalos, P. M.; Romerijin, H. E.; Tuy, H. Recent developments and trends in global optimization. *J. Comput. Appl. Math.* **2000**, *124*, 209.

(40) Deb, K.; Pratap, A.; Agarwal, S.; Meyarivan, T. A Fast and Elitist Multi-Objective Genetic Algorithm: NSGA-II. *IEEE Trans.Evol. Comput.* **2002**, *6* (2), 182.

(41) Srinivas, N.; Deb, K. Multi-Objective Function Optimization using Non-Dominated Sorting Genetic Algorithms. *Evol. Comput.* **1995**, *2* (3), 221.

(42) Rajesh, J. K.; Gupta, S. K.; Rangaiah, G. P.; Ray, A. K. Multi-objective optimization of industrial hydrogen plants. *Chem. Eng. Sci.* **2001**, *56*, 999.

(43) Deb, K.; Agrawal, R. B. Simulated Binary Crossover for Continuous Search Space. *Complex Syst.* **1995**, *9* (2), 115.

(44) Tarafder, A.; Ray, A. K.; Rangaiah, G. P. Application of nondominated sorting genetic algorithms for multi-objective optimization of an industrial styrene reactor. Presented at the second international conference on computational intelligence, robotics and autonomous systems, CIRAS, Singapore, 2003.

(45) Rapaport, I. B. *Chemistry and technology of synthetic liquid fuels*, 2nd ed.; Israel program for scientific translation: 1962.